



PCMDI Report No. 50

**COMPARISON OF THE 200 HPA CIRCULATION IN CSM
AND CCM3 SIMULATIONS & NCEP & ERA REANALYSIS:
SEASONAL CYCLE AND INTERANNUAL VARIATION**

by

James S. Boyle

**Program for Climate Model diagnosis and Intercomparison
Lawrence Livermore National Laboratory, Livermore, CA, USA**

October 1998

**PROGRAM FOR CLIMATE MODEL DIAGNOSIS AND INTERCOMPARISON
UNIVERSITY OF CALIFORNIA, LAWRENCE LIVERMORE NATIONAL LABORATORY,
LIVERMORE, CA 94550**

DISCLAIMER

This document was prepared as an account of work sponsored by an agency of the United States Government. Neither the United States Government nor the University of California nor any of their employees, makes any warranty, express or implied, or assumes any legal liability or responsibility for the accuracy, completeness, or usefulness of any information, apparatus, product, or process disclosed, or represents that its use would not infringe privately owned rights. Reference herein to any specific commercial product, process, or service by trade name, trademark, manufacturer, or otherwise, does not necessarily constitute or imply its endorsement, recommendation, or favoring by the United States Government or the University of California. The views and opinions of authors expressed herein do not necessarily state or reflect those of the United States Government or the University of California, and shall not be used for advertising or product endorsement purposes.

This report has been reproduced
directly from the best available copy.

Available to DOE and DOE contractors from the
Office of Scientific and Technical Information
P.O. Box 62, Oak Ridge, TN 37831
Prices available from (615) 576-8401, FTS 626-8401

Available to the public from the
National Technical Information Service
U.S. Department of Commerce
5285 Port Royal Rd.,
Springfield, VA 22161

Abstract

In this paper the monthly mean vorticity and divergence at 200 hPa are compared from four data sources: The NCEP/NCAR reanalyses 1958 through 1994, the ECMWF (ERA) reanalyses, 1979 through 1994, a NCAR CCM3 integration using prescribed SSTs from 1979 through 1993, and the NCAR CSM 300 year integration. The NCEP, ERA and CCM3 all provide monthly mean data for the period 1979 through 1993. The timescales examined are the annual cycle and interannual variations.

The annual mean vorticity of the ERA and NCEP match very closely. The annual cycle is likewise in good agreement except in the eastern equatorial Pacific and Indian Ocean. Compared to the reanalyses, the models have adequate annual means but suffer in the depiction of the annual cycle in the regions of the jet maxima and in some regions of the Tropics. The CSM appears to inherit errors from the CCM3.

The annual mean divergence evinces a much larger difference between the reanalyses. This is most pronounced in the Tropics, especially over the African and South American land masses. The model simulations also show large differences, with the CSM being an outlier in the tropical Pacific. For many tropical and extratropical locations the annual cycle is not well defined between the NCEP and ERA reanalysis.

The NCEP, ERA, CCM3 and CSM agree with respect to the variance of the monthly mean vorticity. The variance for low pass filtered data is too large in the ENSO regions for the CCM3, but too small for the CSM. Both models tend to underestimate the low frequency variance in midlatitudes.

The ERA has substantially more monthly variance in the divergence than the NCEP data, especially over the tropical South America and Africa and the Dateline. Both models have variance more in line with that of the ERA, and have an anomalous maximum in the eastern Indian Ocean, the CSM much more so. The CSM shifts the maxima in the equatorial Pacific from Dateline seen in the reanalyses to 150E.

The CCM3 appears to be too sensitive to the Equatorial SST anomalies, which may contribute to or exacerbate the poor ocean simulation in the tropical Pacific by the CSM. There are errors in the CCM3 integration which foreshadow, deficiencies in the CSM integration, so the ocean is not solely at fault.

The amount of disagreement between the ERA and NCEP divergence fields on

the time scales of the annual cycle and low frequency variations indicates that this field is poorly defined, and in some regions unknown except for sign.

Introduction

This work will present comparisons of the seasonal cycle climatology and monthly variability of the upper level circulation for the NCAR Climate Simulation Model (CSM, Boville and Gent, 1998) 300 year run, a NCAR Community Climate Model version 3 (CCM3, Kiehl et al., 1998) AMIP type simulation, and the NCEP/NCAR and ECMWF (ERA) reanalysis data sets. This work has several aims. One is to look at the available reanalyses data sets and compare them from a specific perspective. This will provide some idea of the uncertainties still inherent in our knowledge of this aspect of the contemporary atmospheric state. Another purpose is to evaluate the CCM3 and CSM simulations, with respect to the reanalyses data. Finally, this represents an initial attempt to explore the types of variability seen in an extended coupled integration with the new NCAR climate system.

In this work only a very small subset of variables available from the models and reanalyses are considered; the global fields of divergence and streamfunction at 200 hPa for the seasonal cycle and monthly mean variability. This upper level circulation is active in both the Tropics and midlatitudes and enables a global assessment of model performance. Over the globe the 200 hPa level is probably a fair compromise for a level of key activity. It is a bit low in the Tropics and high for the polar regions. Often the upper level dynamics reflect a rough vertical integration of the processes acting in the column below, in this sense it performs a useful diagnostic of overall model performance. A disadvantage is that it is impossible to disentangle all the processes contributing, thus errors can be identified but in most cases cannot be attributed to any specific model shortcoming.

The performance of the model in terms of the characteristics of the annual cycle is a critical test. The most common climatic response of the atmosphere and ocean on short time scales is the seasonal cycle, if the model cannot reproduce this cycle then there remains doubt on the validity on longer time scales. With regard to the longer time scales the temporal extent of the observed data sets is quite limited. The problem of assessing a multiple century model using a data set of less than 40 years of reanalysis data (the present length of the NCEP reanalysis) is statistically intractable. In addition changes in the observing network introduce inhomogeneities that are difficult to take into account. The tact taken here is an attempt to diagnose some of the underlying dynamics to verify if the most prominent variations in the models and observations have a similar physical basis.

The AMIP protocol, Gates (1992), prescribes the time evolving observed SSTs as the boundary condition for atmospheric GCMs. This dictates that the AMIP integrations should share some common characteristics with the reanalyses, which presumably will have similar responses to the varying SST. For diagnosis of a coupled model the emphasis changes, from looking for a specific response to a sequence of prescribed SSTs to looking for similar type of phenomena and responses without regard to specific time sequences beyond seasonally forced variations.

Hurrell et al. (1998) and Boville and Hurrell (1998) show that the CCM3 produces a very reasonable climatology compared to the observations and that the CSM and CCM3 agree closely on most aspects of the atmospheric circulation. Meehl and Arblaster (1998) carry out a close examination of the Asian/Australian monsoon and the ENSO in this CSM integration. They show the model represents most of the major features of the monsoon system and its connections of the tropical Pacific. A time series of the NINO-3 region indicates that the CSM is producing about 60% of the amplitude of the observed variability. Further, the correlations globally with these regions reproduce the main features of the observed variations accompanying ENSO. The CSM displays its largest amplitude ENSO SST anomalies in the western tropical Pacific compared to the observed SST variability maximum in the central and eastern tropical Pacific. This paper is not intended to be a study of the ENSO events in the CSM, but by considering the dominant modes of longer time scale variation in the observations and models the ENSO takes center stage, especially in the years since 1979.

In the next section the reanalyses data sets will be described, followed by a description of the model data. The next two sections compare the seasonal cycles of the data sets and the monthly and interannual variance. Finally, there will be a section on conclusions.

Data

1. Re-analyses

The reanalyses data are available from two sources. The first is the NCEP/NCAR reanalyses described by Kalnay et al. (1996). These data are provided on a 2.5 x 2.5 degree longitude latitude grid and consist of monthly means from 1958 to 1996. The second set is the ECMWF Reanalysis (ERA) described by Gibson et al.(1997). These

data are also on a 2.5 x 2.5 degree grid and are monthly means spanning the period from 1979 to 1993. In the next section a very brief overview of some aspects of these data will be presented in order to establish a background for some of the subsequent analysis. Both the reanalyses are an attempt to eliminate the problem of changing data analysis systems which plagued the operational data sets. Both reanalyses ingest approximately the same observational data and the assimilation models are forced by nearly identical SSTs. Although the reanalyses have a uniform assimilation systems they both suffer from a changing observational network, as stations change and as different remote sensing data are introduced. These changes in input data are convolved with the natural variability making estimates of 'true' variability uncertain.

Figure 1a is a time-longitude plot of the 200 hPa NCEP monthly mean divergence anomaly averaged from 2.5S to 2.5N spanning the years 1958 through 1996. The data have been filtered in time using the 11 point filter of Trenberth(1984) after the seasonal cycle was removed. The Trenberth filter effectively eliminates variations of times scales less than 8 months. There is a change in sign in the predominant anomaly near the dateline, the Greenwich meridian and around 280E in the middle 1970s. At 280E there appears to be two, perhaps three, distinct regimes. The first is from 1958 to about 1973, this period has somewhat lower values of the divergence. In contrast the period from about 1981 to 1996 has a positive offset from the mean. The fact that the transition in equatorial divergence regimes occurs at about 1977 might be attributed to the first introduction of satellite data and other concomitant changes in the observational network, Basist and Chelliah (1995). These changes might have had an impact that altered the nature of the divergence generated by the assimilation system at NCEP. Alternatively, this may represent a real transition, and might indicate that there is an secular change taking place in the circulation. Such changes have been noted by Wang (1995), Zhang et al. (1997), Trenberth and Hurrell (1994), and Trenberth (1995). Figure 1b is the Southern Oscillation Index (SOI) calculated by the NCEP Climate Prediction Center from the observed pressure and Darwin and Tahiti. These data have also been passed through the Trenberth filter. This plot indicates that there is a transition in this index in the middle to late 1970s, with a fairly definitive break occurring about 1978. Presumably, the barometers at Darwin and Tahiti are not influenced by the satellites being launched. In any case, any secular changes in the flow regimes will be convolved with changes in the observational database go-

ing into the reanalyses, making any unambiguous conclusions about the nature of these changes a bit more difficult.

Figure 2 is similar to Fig. 1a, except the NCEP, ERA data are displayed from 1979 through 1994, the period of overlap from the data at hand from ERA and NCEP. If one ignores the amplitude differences, the correspondence of the features is good for the Pacific region, 140E to 280E. This indicates the domination of the ENSO signal linked to the prescribed SST variations. The prescribed SSTs of the two reanalyses are identical for 1982 onward, and are close before that time. The analyses do not agree well outside of the Pacific Basin. The ERA exhibits a greater amount variation than the NCEP data, especially over the African and South American land masses and the Indian Ocean. The poor correspondence of the NCEP and ERA outside of the immediate, active ENSO region, would indicate that a detailed comparison of divergence must be taken with caution. Even over the Pacific the ERA evinces considerable more amplitude in the variations. Evidently, in these data sparse regions the signature of the assimilation techniques and models makes a significant contribution.

Figure 3 is a time longitude plot of the NCEP reanalysis 200 hPa vorticity anomaly averaged from 10N to 20N from 1958 through 1996. This is a region where the response of the vorticity field to the ENSO variations is pronounced and is a region of relative data sparsity. This figure provides a perspective analogous to Fig. 1a but for the rotational dynamics. The regime changes across the 70s seen in Fig. 1 are not as obvious in Fig. 3, although there is a definite transition around 1976 about the Greenwich meridian. Figure 4 is the same as Fig. 3 except for the NCEP and ERA from 1979 to 1994. The correspondence between the two reanalyses for this field is very close, much closer than for the divergence of Fig. 2. Even for some rather minor features outside of the ENSO dominated Pacific Basin, the two analyses agree well. Presumably, this correspondence is a result of the fact that the rotational wind is more closely tied to the observational data and less influenced by the idiosyncrasies of an individual assimilation system and models. At these latitudes the rotational flow is also coupled, at least weakly, to the mass field, making the dynamical constraints on the data assimilation somewhat more effective than on the divergent wind.

As the above plots indicate the analyses of the divergent wind is still subject to a large degree of uncertainty. The ERA and NCEP groups are forthright in pointing out that this field is strongly colored by the assimilation model and that the definitive description of divergence is still a goal to be achieved.

In the following work, the NCEP re-analyses data are divided into periods of varying lengths to best match the methods or verifying data. The prime period being the period 1979 to 1993 where both the ERA and NCEP reanalyses and the CCM3 simulation data are available. For comparison to the 300 year CSM integration, it is desirable to make use of the longer NCEP period, recognizing some possible inhomogeneities in the analyses.

2. Models

The CSM is described by Boville and Gent (1998). The CCM3 is the atmospheric component of the CSM and is described by Kiehl et al. (1998).

The CCM3 simulation data used is for the period 1979 through 1993 using the Reynolds's SSTs after November 1982. The SSTs prescribed for the CCM3 run are monthly means of the data used by the NCEP reanalysis system. Figure 5a is the same as Fig. 2 except for the CCM3 simulation and thus the time only extends through 1993, one year less than Fig. 2. The three ENSO events are quite distinct with amplitudes comparable to the ERA, Fig. 2b, and exceeding those of the NCEP, Fig. 2a. The CCM3 does show more variability outside the ENSO events and region than do the reanalyses. Along 300E (South America) ERA, NCEP and the CCM3 show a large variation in variability and response to ENSOs. Figure 5(b) is the same as Fig. 4 except for the CCM3 data and the time only extends to 1993. Figure 5(b) is quite close in character to the two reanalyses. It would appear that the specification of the SST puts such a strong imprint on this field and in this region that the CCM3 and assimilation models all depict a similar evolution. Both the ERA and NCEP have an indication of some activity at 60E that is not consistently shown in the CCM3.

The CSM data is from the 300 year run, Kiehl et al. (1998). The starting at year 16, the CSM run is sampled for 20 year intervals, to facilitate comparison to available reanalyses, and to assess the modes of variability in these time scales. Where all the 20 year chunks exhibit essentially similar behavior, the 16-35 period will be used, since this is described by Meehl and Arblaster (1998). Figure 6 is the same as Fig. 5(a) except for four 20 year sections of the CSM simulation. It can be seen that the equatorial divergence has a variability level that is similar to the CCM3, but there is a marked lack of the strong anomalies in the Pacific Basin. As discussed by Meehl and Arblaster(1998), the CSM does not produce ENSO variation with nearly a large

enough amplitude. Both the CCM3 and the CSM tend to have enhanced variability in the Indian Ocean region compared to the two reanalyses. The figures for the 10N to 20N vorticity, Fig. 7, are similar in most respects to the CCM3, Fig. 5b, except the eastern Pacific anomalies are reduced in magnitude. The region from 180E to 300E does display some significant anomalies, but these do not appear to be closely linked with any equatorial divergence as is often the case in the observations and CCM3.

Annual Cycle

It would be expected that the seasonal cycle should be quite similar in the two reanalyses. The extensive temporal averaging in generating such a cycle should tend to mitigate any differences. The models should be expected to respond to the seasonal forcing in a realistic fashion. The cycle of the 200 hPa vorticity will be dominated by the waxing and waning of the midlatitude jet streams, while the divergence will reflect the migrations of the Hadley circulations about the Equator, the monsoonal circulations and midlatitude storm tracks.

The seasonal cycle was estimated by performing a harmonic analysis on the monthly mean data. For the NCEP reanalyses the 1979 through 1994 data were used.

a. Vorticity

Figure 8 displays the annual mean and the first harmonic of the NCEP, ERA, CCM3 and CSM for the 200 hPa vorticity for the indicated time periods. Figure 8b displays the actual harmonic dial for the NCEP data, the subsequent corresponding plots are the differences between the respective data set and the NCEP reanalyses. This is done to emphasize what are in some cases, small differences. The harmonic dials are simply subtracted, which confutes the amplitude and phase differences.

Figures 8a,b and 8c,d compare the annual mean and first harmonic of the 200 hPa relative vorticity for the two reanalyses. As might be expected for the rotational component of the wind, the ERA and NCEP are in close agreement. Note that in Fig. 8d, the difference field, the scale is half that of Fig. 8b. The correspondence holds true even in regions of sparse data coverage, such as the Southern Hemisphere and the oceans. The reanalyses mean fields agree to a fairly high level of detail. The annual cycle, Figs. 8b,d, indicates some extended regions of differences in the Eastern Equatorial Pacific and the Indian Ocean where data sparsity may let the differences in as-

simulation system contribute more strongly.

The mean fields of both model simulations, Figs. 8e, g, evince a good agreement with the reanalyses, Figs. 8a,c. Both model runs underestimate the anticyclonic maximum equatorward of the East Asian jet maximum, and enhance the analogous feature over Northern Africa. In some respects, the CSM is actually slightly closer to the observations than the CCM3. The two simulations have a number of differences in common. A strip over northern India oriented east west, both eastern Asia and North America, the northwest Pacific. The CSM appears to have additional problems over the Northern Indian Ocean and Central America and Caribbean. The models have difficulties about the major jet maxima entrance and exit regions.

The problems of the CSM in the Indian Ocean region might well be related to the documented errors in the Equatorial Pacific SST in the simulation, Gent et al. (1998). It is interesting that the error of the CCM3 and CSM in the annual cycle, Figs. 8f,h, are similar in the region of India and southeast Asia, but the CSM has a prominent discrepancy in the Indian Ocean just south of India, not seen in the CCM3. These differences almost appear to add in a linear fashion, the CSM has the same error as the CCM3 and adds an additional problem over the Indian ocean without impacting on the original error.

This does illustrate the possible utility of evaluating the atmospheric component of a coupled model running with prescribed SSTs. The CSM discrepancies could arise from the atmospheric model errors or from the interaction of the other ocean-ice components. Comparing Fig. 8f and 8h, indicates that the CSM inherits some errors from the CCM3 but adds its own. The additional errors might arise due to some synergy amongst the errors of the components.

The percent variance explained by the first two harmonics is shown in Table 1. The models tend to have a slightly higher values for the first harmonic. This is in keeping with the common wisdom that the models have less variability overall so that the annual cycle plays a larger role. However, it appears that if anything that the models here exhibit more variability, indicating that they systematically overestimate the annual cycle.

To illustrate some specific areas of difficulty in the vorticity seasonal cycle, we now present some annual cycle plots of 200 hPa vorticity for specific regions. These locations were chosen based on differences with the NCEP reanalyses. Two twenty year blocks for the NCEP reanalyses are plotted to provide some (albeit meager) per-

spective on the variations amongst the four twenty year blocks of the CSM.

Fig. 9a is the annual cycle of the 200 hpa vorticity for the 4 CSM time blocks, the CCM3, NCEP, and ERA for the 5 degrees latitude by 5 degrees longitude region centered on 130E, 50N. This is over Northern China. It can be seen that the ERA and NCEP are in agreement although there are differences in the months of maximum and minimum, June for NCEP minimum and July for ERA. In the summer months the CSM and CCM3 both follow similar paths, considerably different from the reanalyses. The strong wintertime vorticity values present in this region do not relax nearly enough during the summer months in the models. The reanalyses have values near zero while the models retain almost a wintertime intensity. Figure 9b is for the region about 270E, 20N, this is located over Central America. In this region the CSM and CCM3 have different behavior from each other and the reanalyses. The reanalyses agree with each other rather closely while the CSM and CCM3 have opposite signs in the summer. The CSM appears to capture the nature of the reanalyses variations, but has an amplitude that is much too great during the summer months. This behavior appears unique to the CSM, and may be related to the Equatorial ocean problems. Figure 9c is the plot for 270E, 40N, located over the Eastern US. In this region the shape of the annual cycle is similar for all the data but the models tend to overestimate the summer minimum. Figure 9d is for 300E, 50N which is the location of the mean vorticity maximum on the eastern side of North America. The models considerably over estimate the secondary summer maximum indicated by the reanalyses. This is similar behavior to Fig. 9a which is in an analogous position on the eastern side of the Asian continent. The CCM3 and CSM shift the phase between each other for the summer maximum. Figure 9e is for the region 350E, 10N, located over the African Guinea coast. Here the models overestimate the late summer maximum seen in the reanalyses. Although the CCM3 and CSM disagree on the month of the peak, being July and August, respectively, they clearly agree on the anomalously large amplitude. This is in contrast to the behavior over Central America, Fig.9b, where the CCM3 and CSM showed separate differences from the reanalyses. The problems in Central America might well be due to the documented errors in the Pacific Equatorial SST developed early in the CSM integration, Gent et. al. (1998). Yet these figures indicate that not all Equatorial problems can be linked to this weakness. Evidently, the characteristics off the Equatorial African coast are at least in part intrinsic to the atmospheric model and are not completely altered in the coupled simulation.

b. Divergence

Figure 10 shows the annual mean of the monthly averaged 200 hPa divergence for the NCEP, ERA, CCM3 and CSM and the first harmonic for the NCEP and the difference from NCEP for the other fields. The reanalyses fields for this variable are strongly influenced by the assimilation model formulation and performance as well as differences in the treatment of the satellite data. Although constrained by the prescribed SSTs and the observed data, these constraints on the assimilation are particularly weak for the irrotational wind, especially in the Tropics where the geostrophic relations are not strong and conventional data are sparse.

There is fair agreement in the annual mean between the two reanalyses. Not to the degree that was seen for the vorticity, but there is a general correspondence for most of the features with some variations in location and magnitude. The models do a fair job of copying the observations, with some regions of differences. The CSM suffers from the presence of a cold tongue of water along the equator. The error in the ocean simulation is clearly manifested at the dateline, although the Pacific simulation of the CSM has many characteristics not unlike the NCEP fields. Both models tend to substantially overdo the convection in the Western Pacific with the CSM placing an emphatic divergence center too far east at about 120E. The CSM has strong maxima over South America and Africa. Prominent possible problem spots appear to be the Indian Ocean, Arabian Sea, Bay of Bengal regions. The CSM especially tends to have a maximum just northeast of Madagascar, and is too weak in the Bay of Bengal. There are also apparent artifacts due to high terrain over the Andes and Tibetan Plateau these are perhaps at least partially due to the interpolation from hybrid sigma to pressure coordinates.

Figure 10b and 10d compare the first harmonic of the divergence field of NCEP and ERA. Note that the figures other than NCEP depict the difference of the particular field minus NCEP. Here the *same* scaling is used for the difference fields as for the whole field. In Fig. 10b the ERA and NCEP have the largest differences in the Tropics where the first harmonic of this field has its largest amplitude. There are differences in amplitude and phase. If the difference dial were to be pointing in the same direction as the NCEP dial then the difference, if non-zero is attributable to just an amplitude discrepancy. On either side of the Equator, this is generally a phase differences. This is understandable as small differences in the movement and strength of

the ITCZ as it moves following the sun can lead to differences seen in Fig. 10d. The CCM3 differences are not a good deal larger than those of the ERA reanalyses. Discounting the regions over the Tibetan Plateau and the Andes, a region of large differences is in the Equatorial region from Greenwich to about 150E. The CSM has this as a problem area along with the band on either side of the cold tongue across the Pacific. One might be tempted to attribute the CSM discrepancies in the Indian Ocean due to its documented SST shortcomings in the tropical Pacific. However, the CCM3 fields indicate that this may be an intrinsic feature of the atmospheric model and is perhaps exacerbated in the CSM. Both the CSM and CCM3 have an interesting differences on the eastern Asia coast, both have a difference in phase, there is a similar problem on the eastern North American region. The CSM has a spectacular center northeast of Madagascar, some lesser ones at 240E, 20S, to the west of Central America, and over Northern China and the dateline. Again there are some inklings of the CMS errors in the CCM3 fields.

The percent of variance explained by the first two harmonics of the divergence is shown in Table 2. The percent explained by the first harmonic in Table 2 have dropped by a substantial amount from the analogous values for the vorticity in Table 1. The decrease for the models is greater than the reanalyses. In this case the reanalyses and models have about the same values. The values of the second harmonic are about the same as those for the vorticity.

Figure 11 presents some annual cycle plots for the 200 hPa divergence at specific locations for the CCM3, CSM (four twenty year time blocks), the NCEP (two twenty year time blocks + mean) and the ERA.

Figure 11a is over 115-125E, 10S-10N which is a position over the Maritime continent and near the CSM equatorial maximum. The clear bias of the CSM in overestimating the divergence in this region is apparent from April to September. The lack of agreement between the two reanalyses during the winter makes absolute validation problematical. It's curious to note that the ERA curve appears to be the outlier. The CCM3 shows a tendency to have a larger divergence during the same months as the CSM, although its peak is in June rather than April-May as in the CSM. Note that there is not a small amount of variation in this field for the four blocks of the CSM, somewhat more than the two blocks of NCEP. Figure 11b is for 140E to 170E and 10S to 10N which is over the oceanic 'warm pool region'. Here the impact of the too cool SSTs of the CSM is evident in that the CSM underestimates the divergence just about

out of phase with Fig 11a. Here too the reanalyses and CCM3 do not agree to any large extent, the mean values of the CCM3 and ERA probably being closer to each other than NCEP and ERA. Figure 11c is for a region in the tropical eastern Pacific, 240E, 10N. The CSM is out of phase with NCEP but from April to June the CSM and ERA both show a strong increase while the NCEP decreases. The CCM3 has little amplitude, weakly agreeing with the CSM after June. The ERA has a much greater divergence from May to December compared to the NCEP. In October and November the ERA and CSM agree more closely than the two reanalyses. Figure 11d is over the eastern United States centered at 270E, 40N. This region shows a large difference in the behavior of the NCEP divergence for the two time blocks, as does the different periods of the CSM. The NCEP period coincident in time with the ERA shows good agreement, whilst the earlier period has a large difference from June to December. This may be an indication that the secular change discussed previously, may be manifested even in the annual cycle of the two time periods in midlatitudes. In the summer months the models tend to overestimate the divergence, although there is quite a bit of variation in the CSM blocks. Fig 11e is for the region northeast of Madagascar located at 60E, 10S. The anomalously large value of CSM divergence in this region is seen to have essentially all its contribution from January, February and March. This large peak in strong contrast to the staid behavior of the two reanalyses. The CCM3 has too much divergence compared to the reanalyses in the Spring. Perhaps, the CCM# and CSM errors are only related in the sense that the Indian Ocean is difficult and is a prime location for errors to be prominent. Figure 11f is located over the Bay of Bengal at 90E, 10N another region of consistent model error. Here it is seen that the CCM3 and CSM agree to disagree with the reanalyses from April to October, while the CSM proceeds on its own to anomalous convergence for December, January, February and March.

Standard Deviations

In contrast to the preceding sections which dealt with mean states of the atmosphere, the next section will focus on variability. The standard deviation will be presented for filtered and unfiltered data, the seasonal cycle being removed.

a. Vorticity

Figure 12 is the standard deviation of the 200 hPa monthly mean vorticity of the four data sets for the time periods considered with just the annual cycle removed. The

maxima in all the data sets correspond to regions of jet stream and storm activity in the subtropics and midlatitudes. These fields are dominated by the mid-latitude jets exit / storm track structures. The variability of these features are adequately analyzed and apparently fairly well modeled. The CSM does not capture the larger values which encroach on the equatorial pacific at about 120W as in the CCM3 and reanalyses. In the North Pacific, the models seem to have less of an east west extension than do the reanalyses. The overall standard deviation levels match up fairly closely for all the data sets, the reanalyses generally having slightly larger maxima.

Figure 13 is the standard deviation of the time series of 200 hpa vorticity with the seasonal cycle removed and filtered with the Trenberth filter to remove variations of less than 8 months. The cellular structures oriented north south in the Pacific basin are typical of ENSO variations. The CCM3 has too strong response in the Equatorial Pacific but is more in line with the reanalyses in the Northern Pacific. The CSM underestimates the ENSO variations, it does not have the near equatorial maxima seen the other fields but rather two maxima farther poleward in the Pacific near 20N. In the Southern hemisphere the CSM misses any equatorial maximum in the Pacific almost entirely. It is curious that this CSM chunk does have some of the “far field ‘response of ENSO, for example of the Southern US while completely missing that of the southern hemisphere.

b. Divergence

Figure 14 presents the standard deviation of the monthly mean 200 hpa divergence with the annual cycle removed. The correspondence seen in the analogous vorticity fields, Fig. 12, has somewhat diminished. The focus of activity has shifted from the extratropics to the tropics. The NCEP reanalyses amplitude is much reduced from that of the ERA in virtually all regions. There is only broad agreement as to the regions of greatest activity. The ERA is very active over South America and Africa. This might be due to the treatment of land surface processes in the assimilation model, promoting more penetrative convection. The typical ENSO signature variation at the dateline is some three times larger in ERA. The CCM3 more closely resembles the ERA rather than NCEP. In general the CCM3 is even more variable. The relative minima seen in both the NCEP and ERA west of South America, North America and Africa is missing in the CCM3. There is a large maximum in the western Indian Ocean. The CSM shifts the Dateline maximum well the west to 150E, and enormously

amplifies the Indian Ocean maxima at 60E from the CCM3 values. Even given the severe problems with the Pacific SSTs the CSM appears to have elements in common with the CCM3. Both have greater variability than either reanalyses.

Figure 15 presents the standard deviation of the monthly mean 200 hpa divergence with the annual cycle removed and filtered with the Trenberth filter. Comparing 14 a,b and 15a,b it can be seen that the lower frequency variations make a significant contribution the totals in Fig. 14. The comparison of the NCEP and ERA proceeds much like the preceding field, however the amplitude of the ERA is even larger all along the Equator. The ERA has much greater values than the NCEP and this is especially true over Africa and South America. The CCM3 matches the ERA fairly well over the ENSO region of the Tropical Pacific but has somewhat lower variability over the continents albeit greater than the NCEP. The CSM has the Tropical Pacific maxima squeezed up against 150E, the effects of the anomalously cold Equatorial Pacific water are quite in evidence. In the CSM the activity in the Indian Ocean is enhanced with respect to the CCM3 and has a band which joins the separate centers of the ERA. Africa and South America have less variation than the CCM3, although even these are generally above the NCEP. The whole of the Pacific east of the Dateline is quiescent in the CSM compared to the other data.

Conclusions

In this paper the monthly mean vorticity and divergence at 200 hPa are compared from sources: the NCEP/NCAR reanalyses, the ECMWF (ERA) reanalyses, a NCAR CCM3 integration using prescribed SSTs, and the NCAR CSM 300 year integration. The NCEP, ERA and CCM3 integration all provide data for the period 1979 to 1993. The aspects of the vorticity and divergence examined were the annual mean, the annual cycle, the interannual variability and the low frequency interannual variability using a low pass filter to emphasize variations greater than 8 months.

The ERA and NCEP reanalyses are for the most part in good agreement with respect to the vorticity (rotational wind). This is true for the mean fields as well as the variances, and annual cycle. The models, CCM3 and CSM, both produce a very credible simulation of the vorticity, but both contain discrepancies which are beyond that expected from normal variability. These errors are largest about the regions of the midlatitude jet maxima, indicating a limitation in the models seasonal oscillation in

strength and position of the major jet cores. These problems occur in regions such as East Asia and North America where the observations are adequate to define the observed circulation. Over Eastern Asia at 50N the annual cycle of vorticity is substantially underestimated, for example. Many of the CCM3 errors are evident in varying degrees in the CSM integration, which has some additional shortcomings of its own. The interannual variability in vorticity is captured by the models, only a bit underestimated in the observed maxima regions of the North Pacific and North Atlantic. The low frequency variability (< 8 months) which is dominated by the ENSO type patterns, is seriously misrepresented in the CSM, this has been previously noted by Meehl and Arblaster (1998). The CCM3 has a substantially stronger variability in the Equatorial Pacific than the NCEP or ERA analyses, clearly overdoing the ENSO signal.

The divergence fields of the reanalyses evince considerably more difference than the vorticity. The discrepancies are largest in the Equatorial regions where the divergence has its largest mean values and the data tend to be sparse. Even so the reanalyses do have the major centers in similar locations but there is considerable discrepancy in details and magnitude. The low frequency variability in the ERA is much larger than the NCEP. The ERA has prominent centers over Africa and South America virtually absent in NCEP. The models show large differences with each other and the reanalyses, although again there are errors of the CCM3 which are propagated to the CSM. The CSM ocean suffers from an anomalous cold tongue across the Equatorial eastern Pacific. A consequence is that the Pacific equatorial divergence in the model is clearly suppressed. Even so, both models show a marked tendency to have an extreme divergence center in the equatorial western Pacific. This center is of comparable magnitude in both models but much farther west in the CSM. Examination of individual points of the seasonal cycle of divergence indicate the considerable uncertainty that still exists in determining the divergence field.

In many respects the current CCM3/CSM do produce a satisfying climatology, but as the models are being used to detect ever more subtle climate effects, the demands on the fidelity of the models proceeds apace. It could be seen from the results here that some of the errors of the CCM3 carry over to the CSM. The Indian Ocean is a region which has considerable variation. An interesting fact is that the models tend to be too variable on the interannual time scale compared to the observations.

The observations, as represented by the reanalyses, indicates that not all aspects

of the 200 hPa circulation can be defined with confidence. This is especially true of the divergence. The shortness of the available data record and disparities among data assimilation system preclude very detailed comparisons. The differences in the variability of the most basic fields and short and longer time scales indicates the need for further research into the reasons for the discrepancies. Are the differences solely due to the models used in the assimilation, or are other analysis techniques contributing? Can these differences be resolved to enable a more definitive assessment of the atmospheric state? It would appear that data assimilation experiments need to be carried out to try and make some estimates of the impact of the changing input data and uncertainties in the boundary conditions of the assimilation (SSTs).

As the models improve sweeping generalizations become less applicable. The CSM often overestimates the amplitude of the seasonal cycle, but this is not globally true. The Tropics remain a problem area, but as shown there is some difficulty in the simulation of the vorticity in the midlatitudes of eastern Asia. The errors of the Equatorial Pacific Ocean will be addressed in the current version of the CSM ocean model. In all likelihood, the most egregious errors of the CSM noted here will be alleviated by the improvement of the ocean component. This will not be a cure all, for example the errors in the Indian Ocean might be attributed to the ocean difficulties but are already evident in the CCM3 computations.

Acknowledgments. The generosity of the NCAR CSM modeling group in making their data available is greatly appreciated. Special thanks to Maurice Blackmon and Dennis Shea of NCAR for facilitating access to the data. This work was performed under the auspices of the Department of Energy Environmental Sciences Division by the Lawrence Livermore National Laboratory under contract W-7405-ENG-48.

References:

- Basist, A. N. and M. Chelliah, 1997: Comparison of tropospheric temperatures derived from the NCEP/NCAR reanalysis, NCEP operational analysis, and the Microwave Sounding Unit. *Bull. Amer. Met. Soc.*, **7**, 1431-1447.:
- Boville, B. A., and P. R. Gent, 1998: The NCAR Climate System Model, Version One., *J. Climate*, **11**, 1115-1130.
- Boville, B. A., and J. W. Hurrell, 1998: A comparison of the atmospheric circulations simulated by the CCM3 and CSM1., *J. Climate*, **11**, 1327-1341.
- Kalnay, E. M., M. Kanimitsu, R. Kistler, W. Collins, D. Deaven, L. Gandin, M. Iredell, S. Saha, G. White, J. Woolen, Y. Zhu, M. Chelliah, W. Ebisuzaki, W. Higgins, J. Janowiak, K. C. Mo, C. Ropelewski, J. Wang, A. Leetma, R. Reynolds, R. Jenne and D. Joseph, 1996: The NCEP/NCAR 40-year reanalysis project. *Bull. Amer. Met. Soc.*, **77**, 437-471.
- Meehl, G. A. and J. M. Arblaster, 1998: The Asian-Australian Monsoon and El Nino Southern Oscillation in the NCAR Climate System Model. *J. Clim*, **11**, 1356-1385.
- Kiehl, J. T., J.J. Hack, G. B. Bonan, B.A. Boville, D. L. Williamson, and P. J. Rasch, 1998: The National Center for Atmospheric Research Community Climate Model: CCM3., *J. Climate*, **11**, 1131-1149.
- Hurrell, J. W. , J. J. Hack, B. A. Boville, D. L. Williamson, and J. T. Kiehl, 1998: The dynamical simulation of the NCAR Comunity Climate Model Versin 3 (CCM3). *J. Climate*, **11**, 1207-1236.
- Gates, W. L., 1992: AMIP: The atmospheric model intercomparison project. *Bull. Amer. Meteor. Soc.*, **73**, 1962-1970.
- Gibson, J. K., P. Kallberg, S. Uppla, A. Hernandez, A. Nomura, and E. Serrano, 1997: ECMWF Re-Analysis Project Report Series. 1. ERA Description. 66p.
- Trenberth, K., 1984: Signal Versus Noise in the Southern Oscillation, *Mon. Wea. Rev.*, **112**, 326-332.
- Trenberth, K. E., 1990: Recent observed interdecadal climate changes in the Northern Hemisphere, *Bull. Amer. Meteor. Soc*, **71**, 988-993.
- Trenberth, K. E. and J. Hurrell, 1994: Decadal atmosphere-ocean variations in the Pacific., *Clim. Dyn*, **9**, 303-319.
- Trenberth, K. E., 1995: Atmospheric circulation changes. *Clim. Change*, **31**, 427-453.
- Wang, B., 1995: Interdecadal changed in El Nino onset in the last four decades. *J.*

Clim.,**8**,267-285.

Zhang, Y., J. M. Wallace and D. S. Battisti, 1997: ENSO-like interdecadal variability:1900-93, *J. Clim.*, **10**, 1004-1020.

Table 1: percent variance explained by harmonics for 200 hpa Vorticity

Data set	First Harmonic	Second Harmonic
CCM3	32	8
CSM 16-35	33	6
CSM 80-99	35	7
ERA	28	5
NCEP	29	6

Table 2: percent variance explained by harmonics for 200 hpa Divergence

Data set	First Harmonic	Second Harmonic
CCM3	17	6
CSM	19	6
CSM	19	7
ERA	17	4
NCEP	20	5

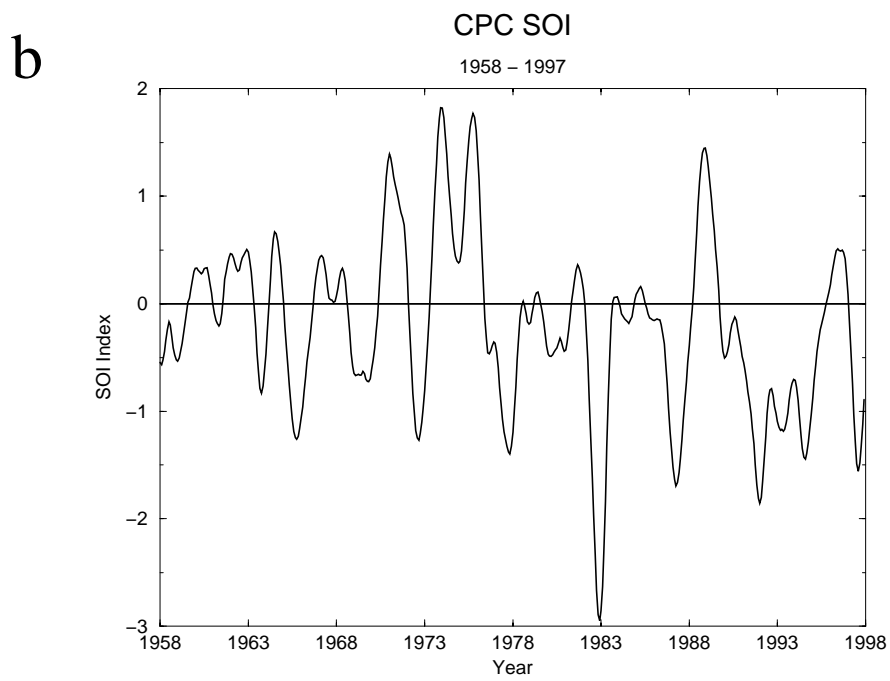
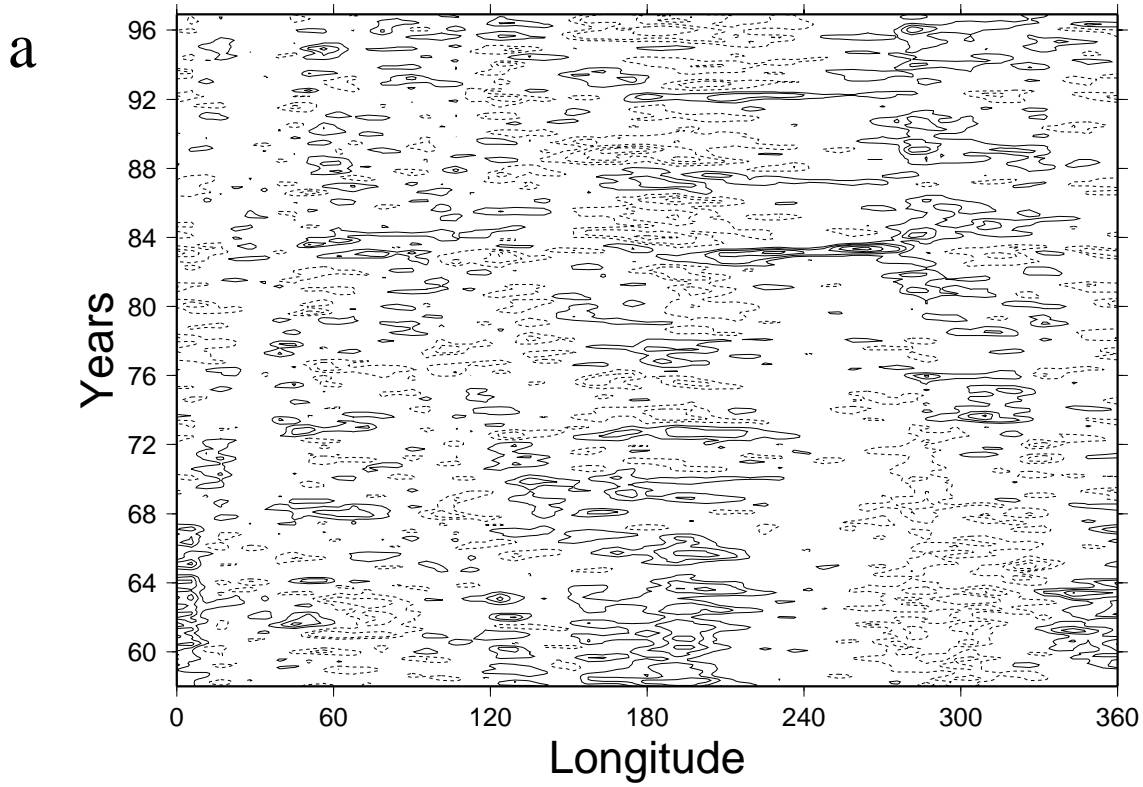


Figure 1. (a) and (b).

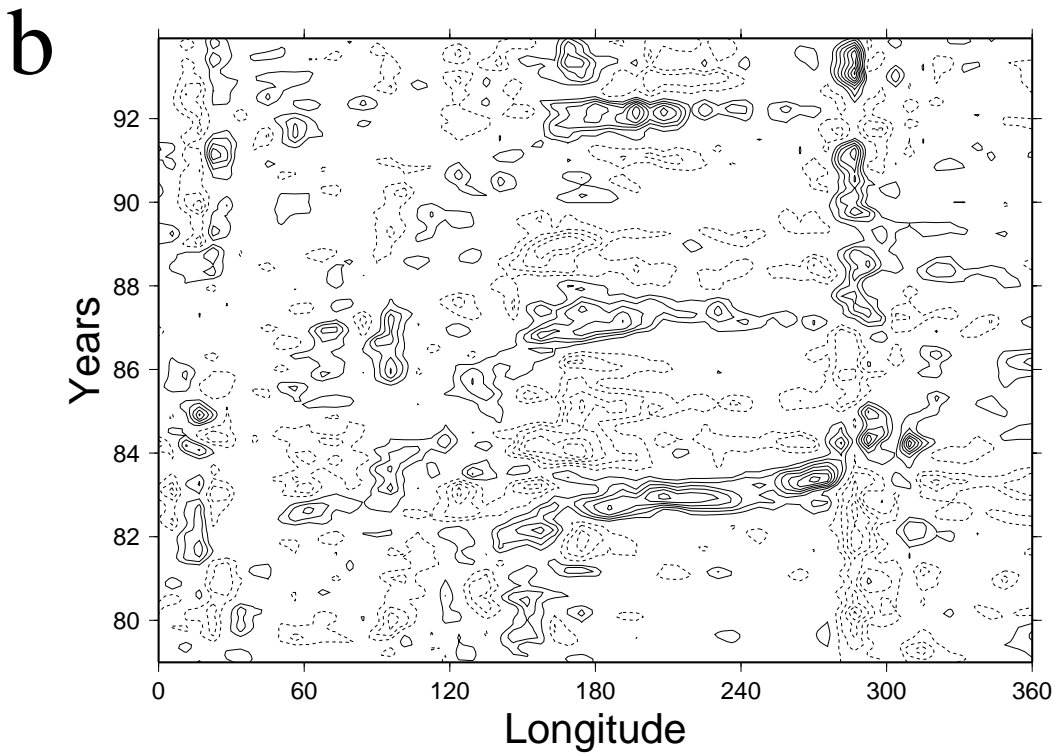
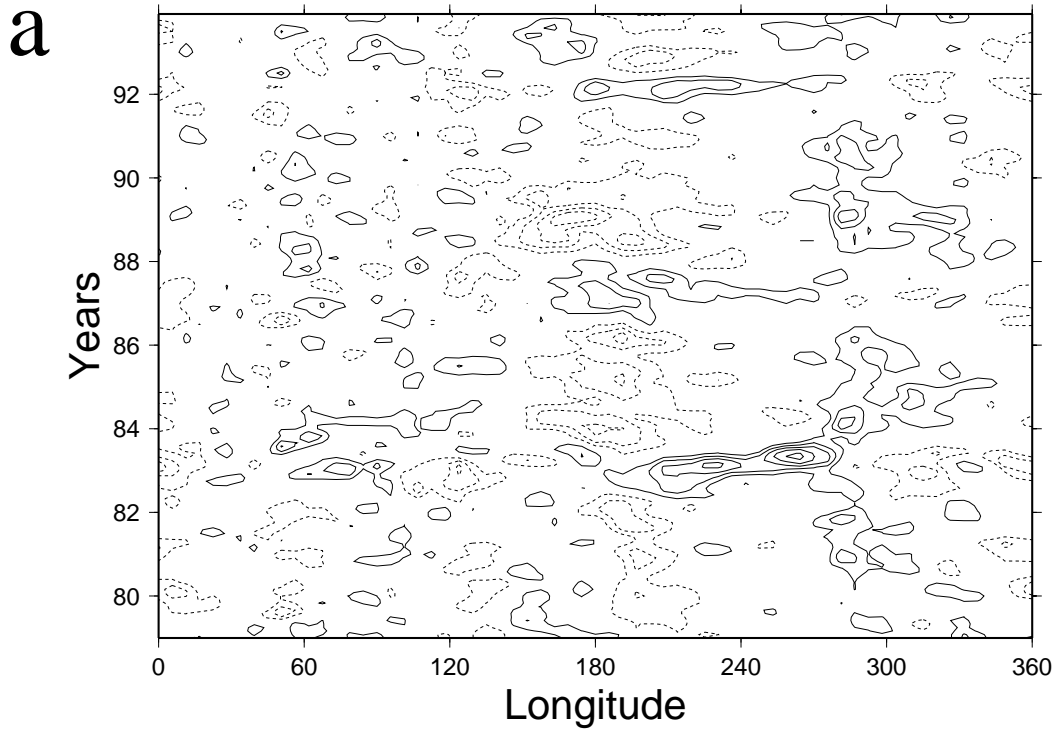


Figure 2.. (a) and (b).

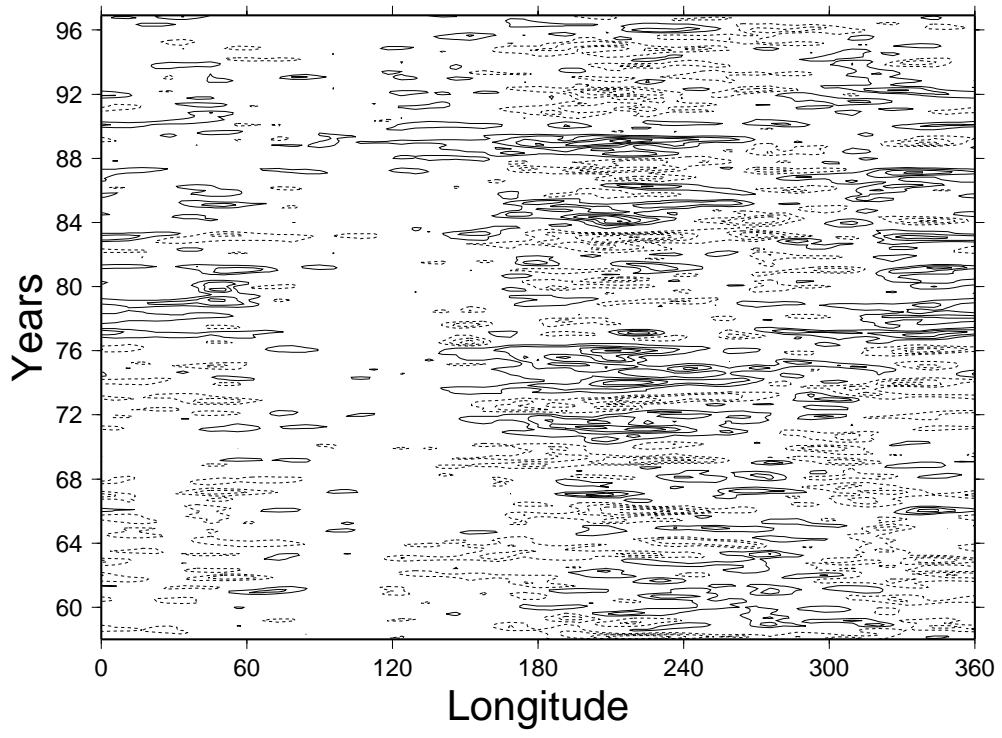


Figure 3.

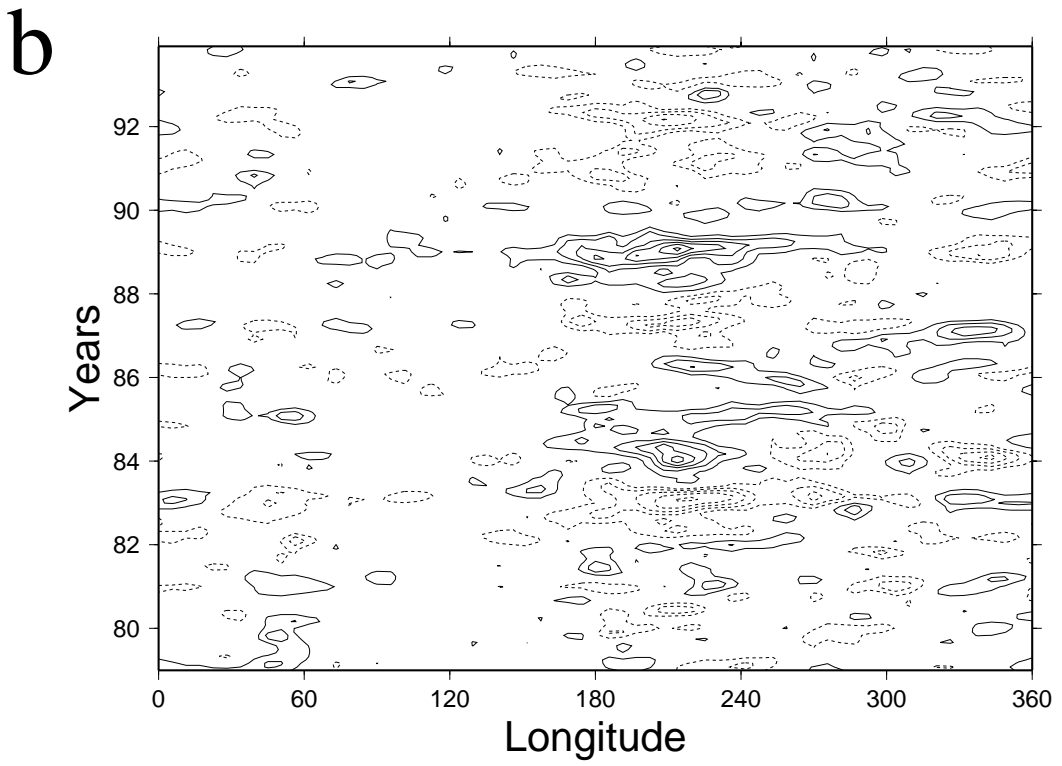
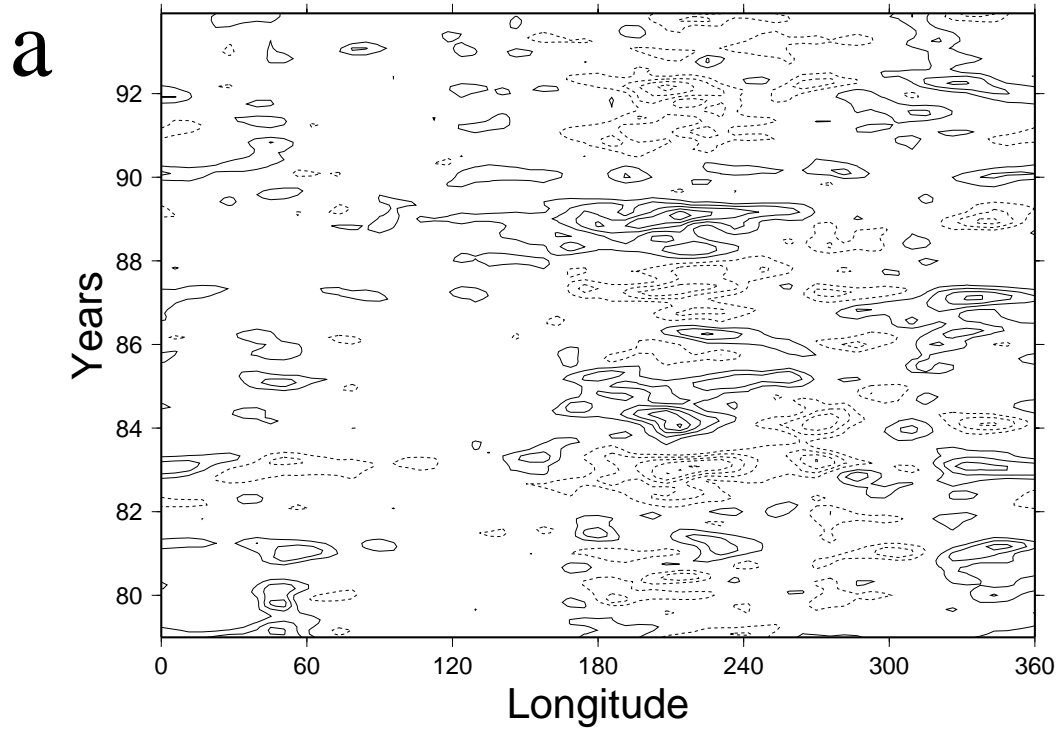


Figure 4. (a) and (b).

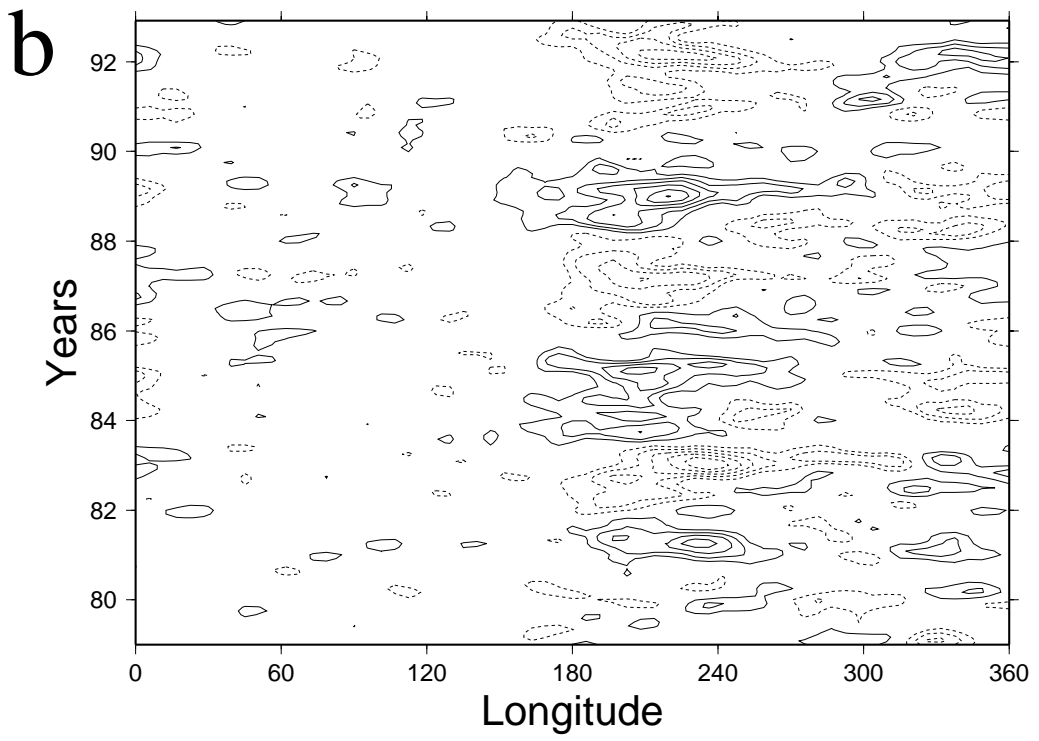
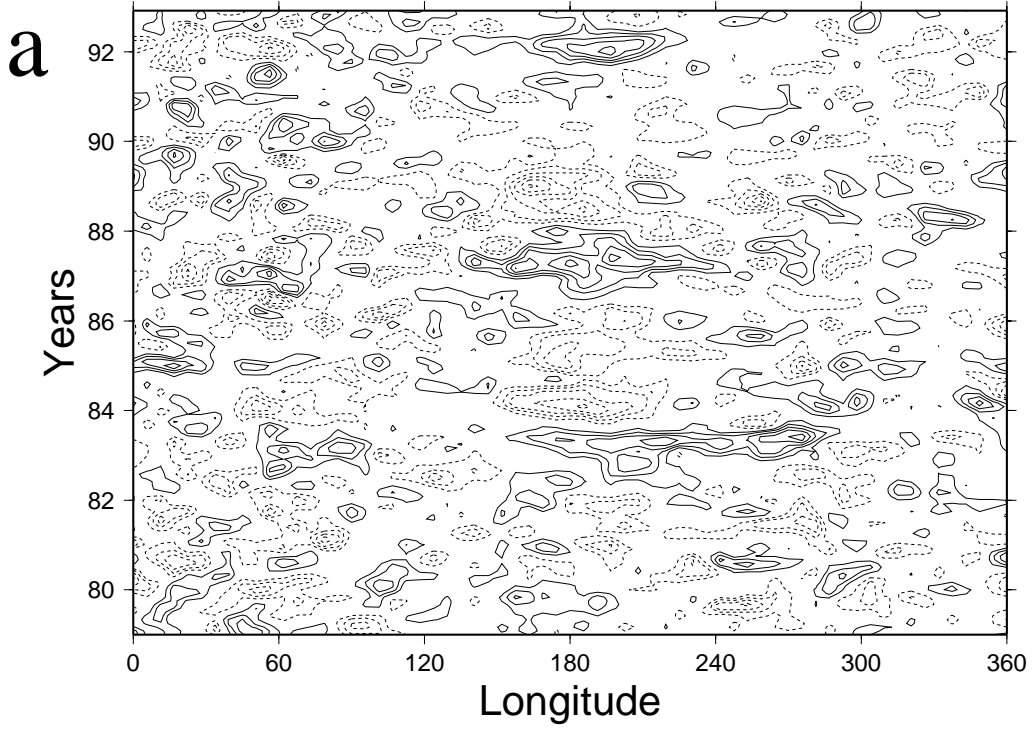


Figure 5. (a) and (b).

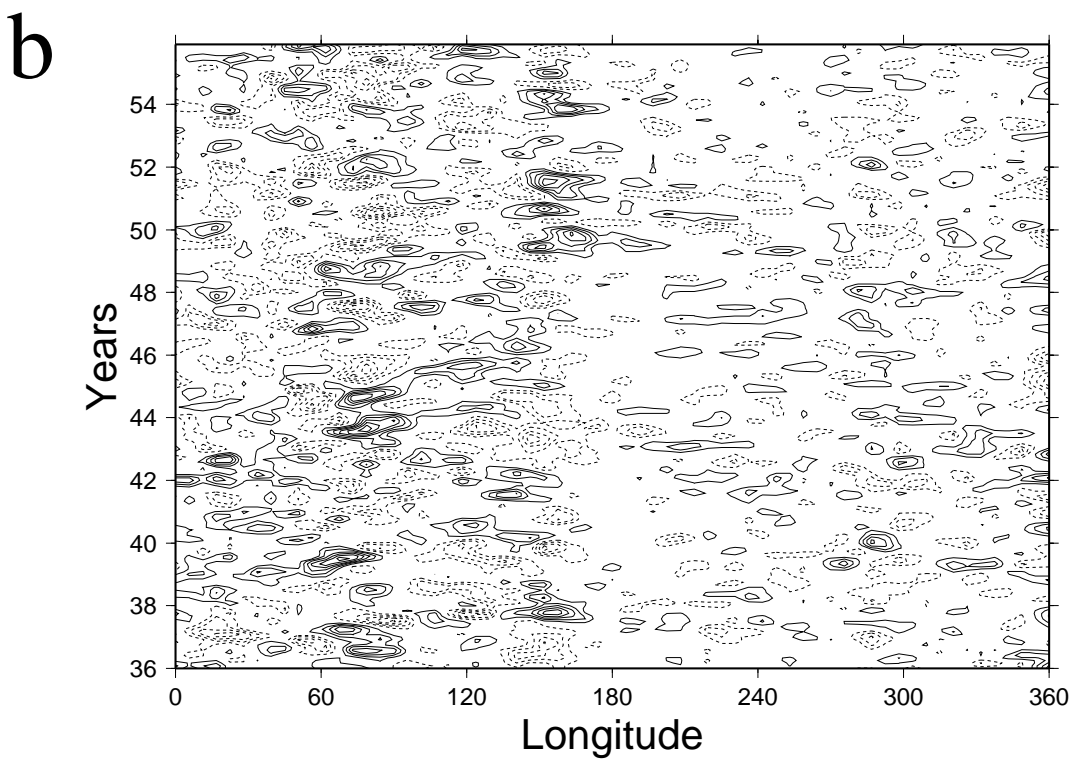
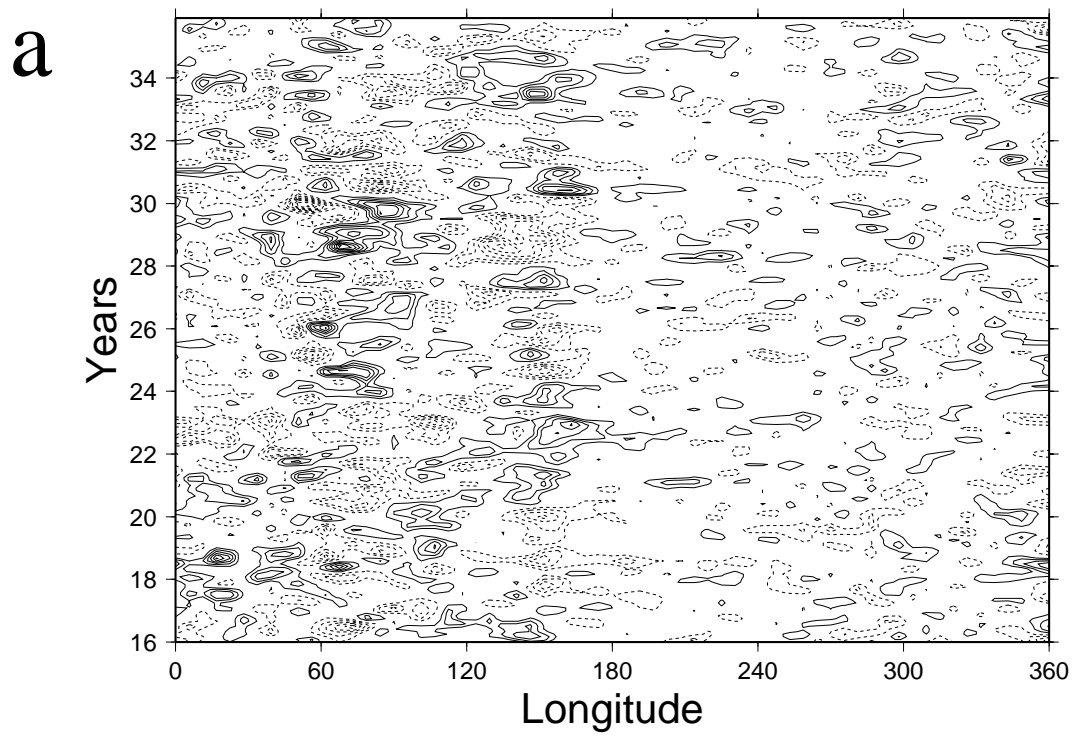


Figure 6. (a) and (b).

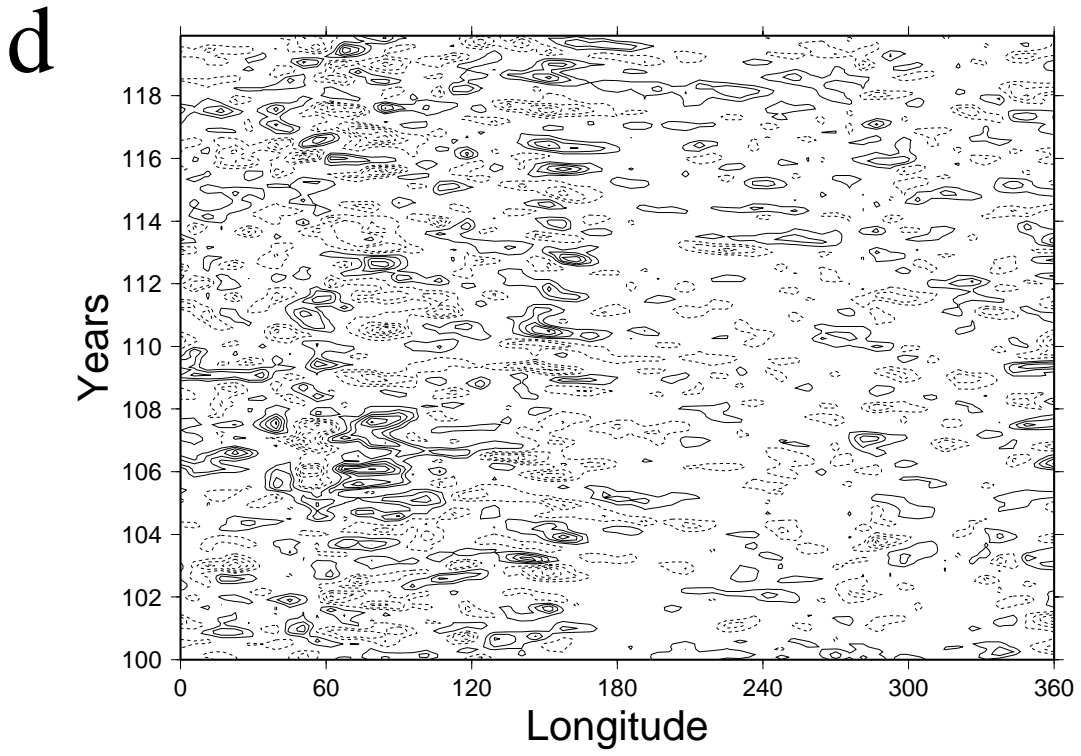
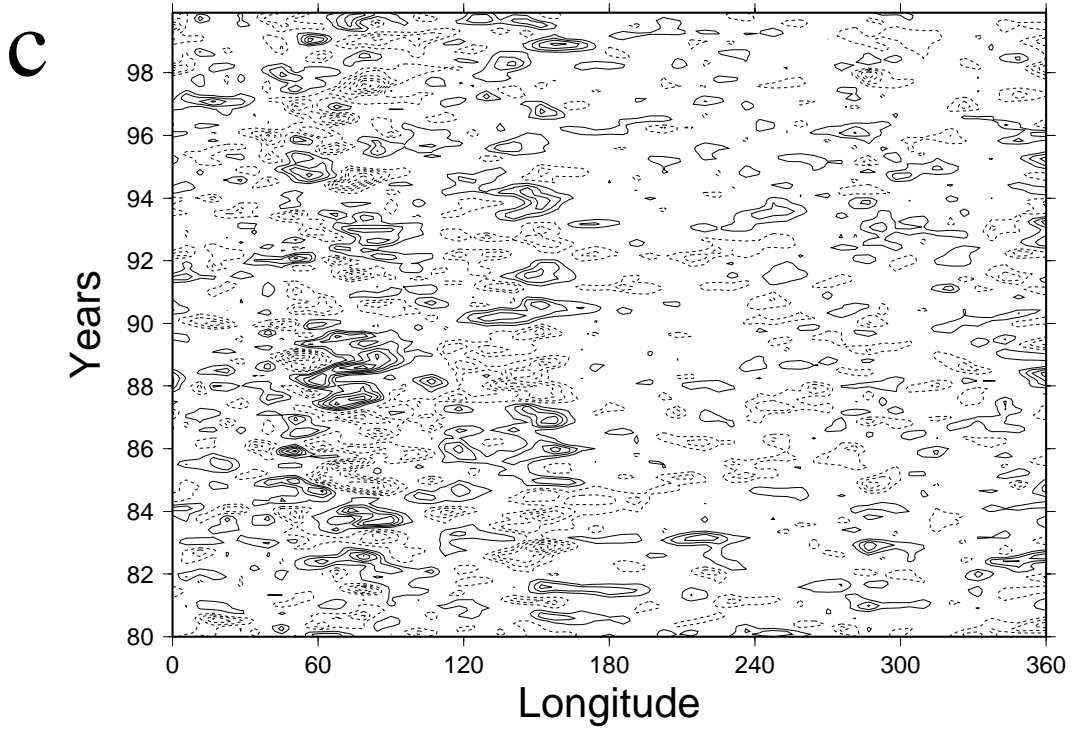


Figure 6. (c) and (d).

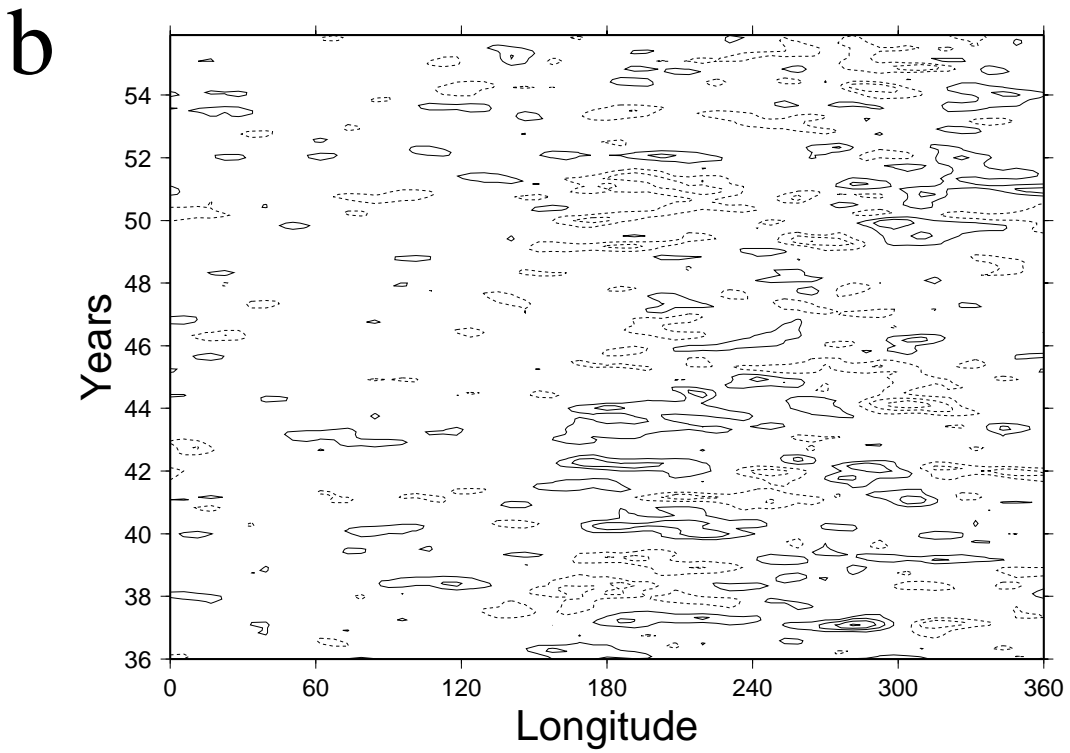
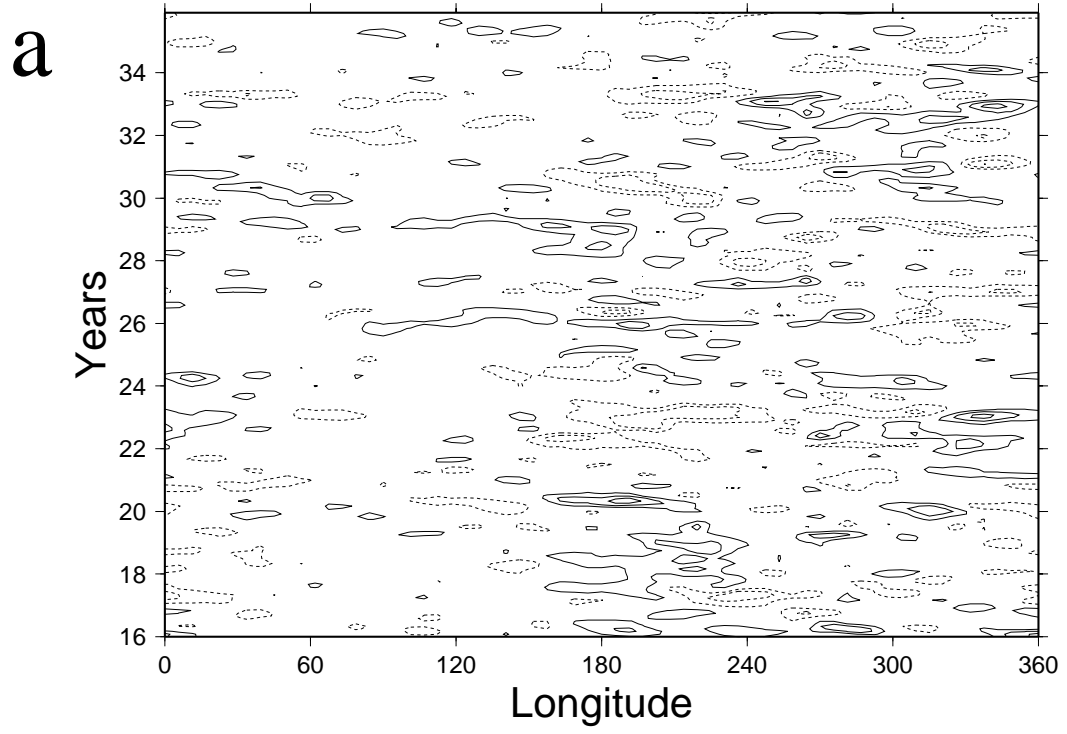


Figure 7. (a) and (b).

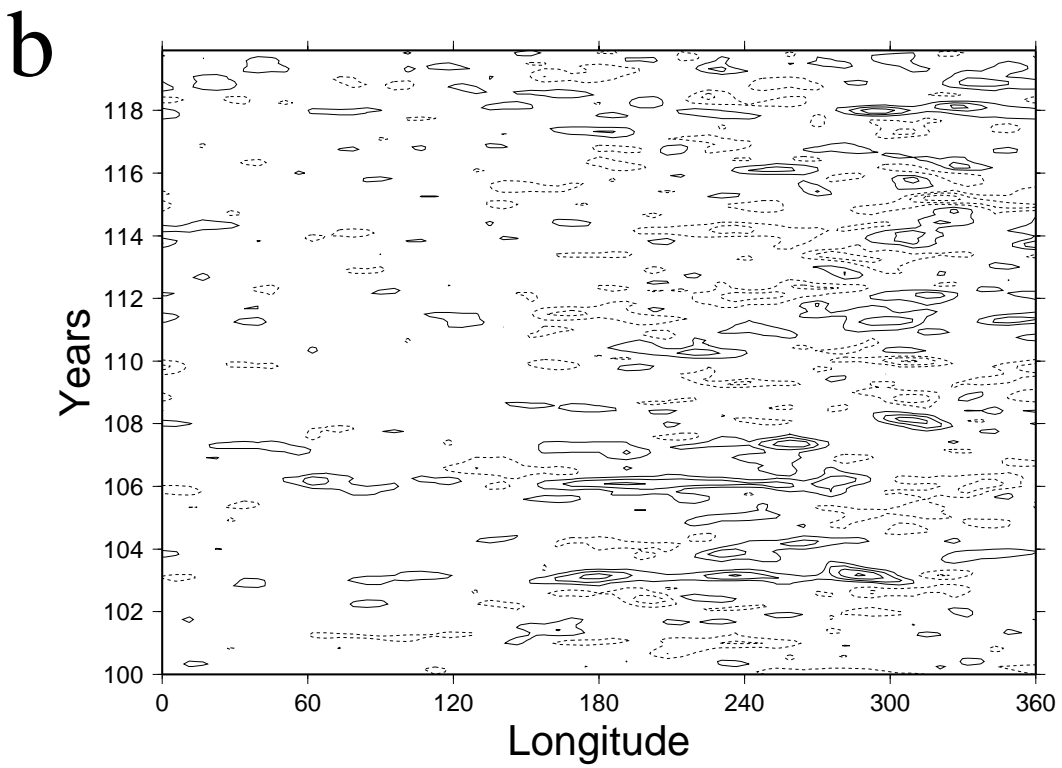
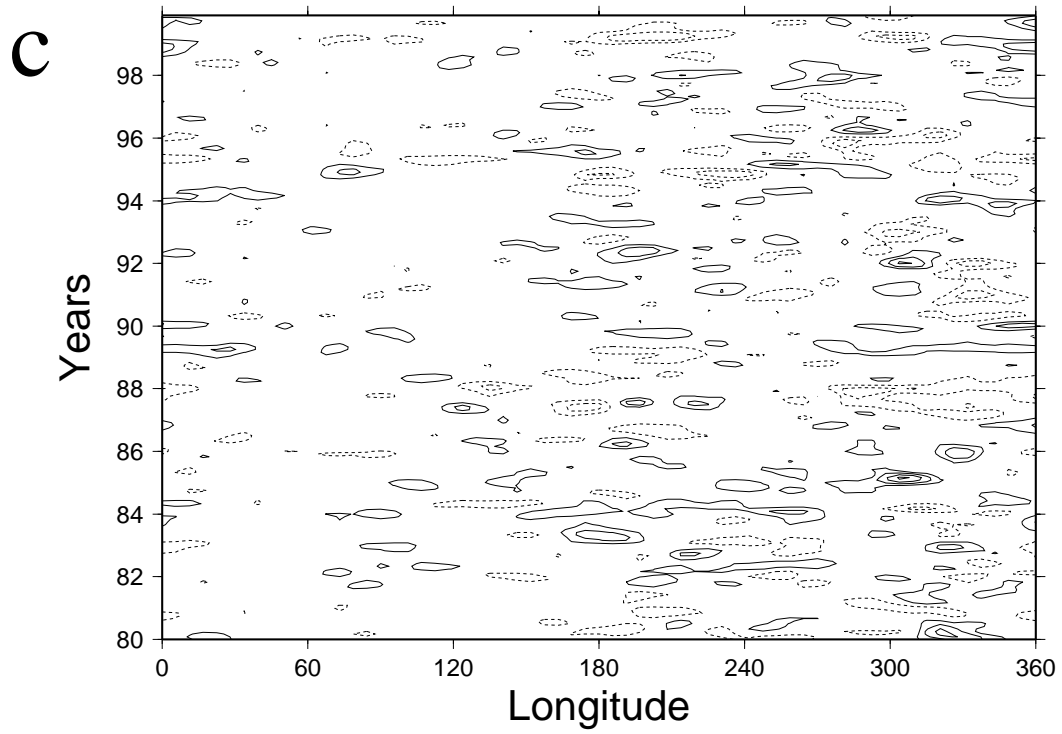


Figure 7. (c) and d).

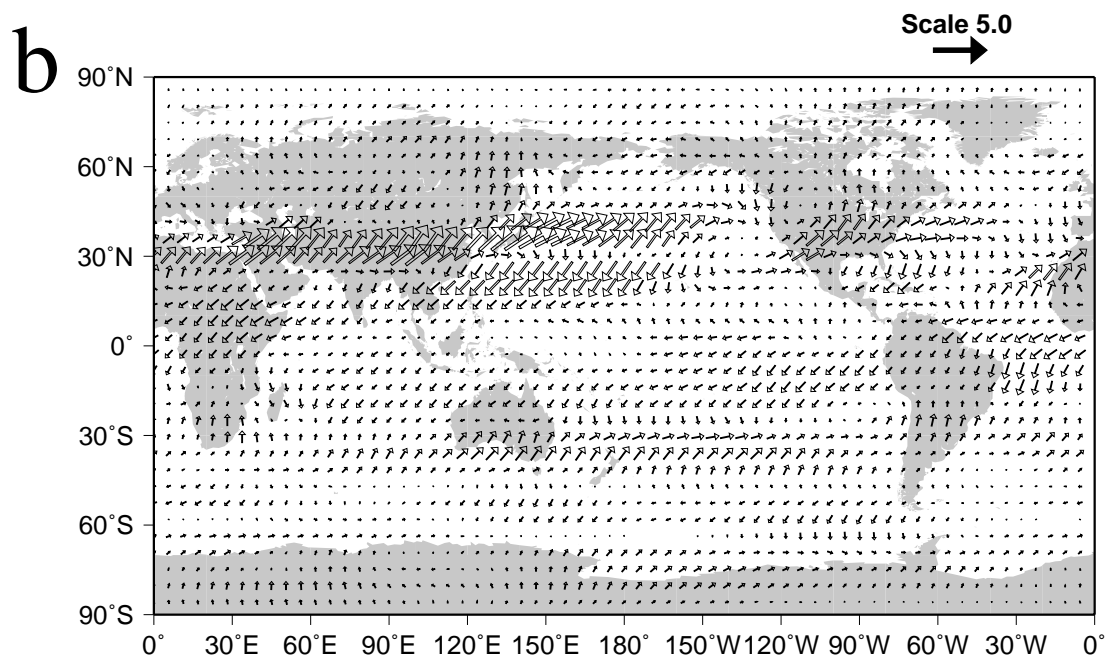
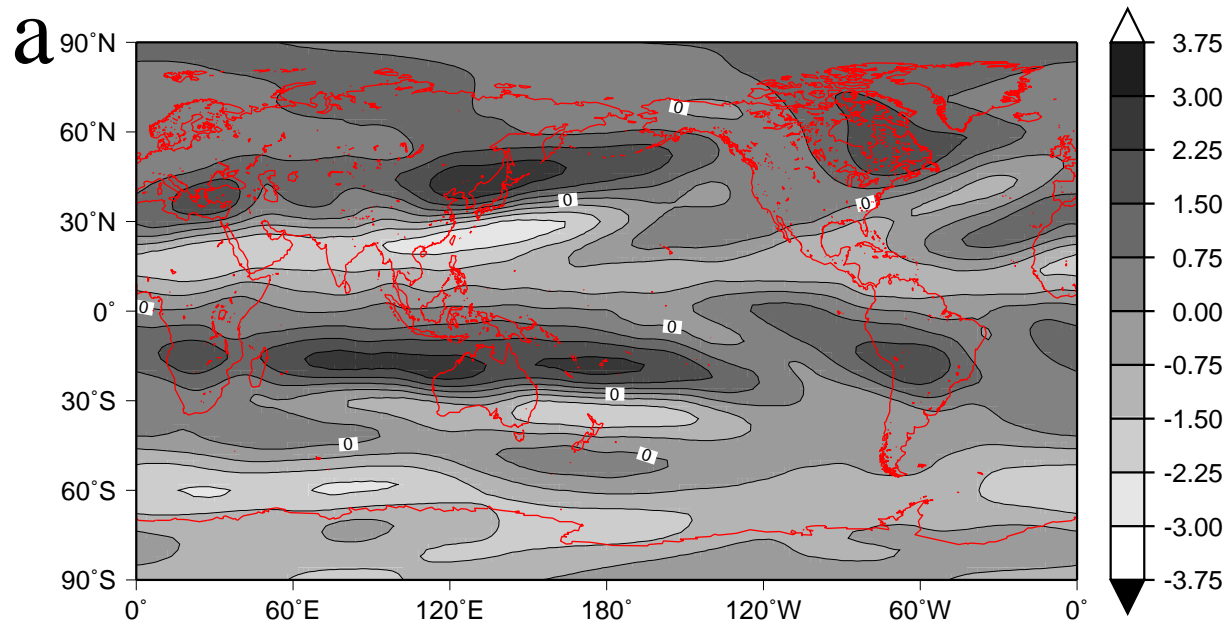


Figure 8. (a) and (b).

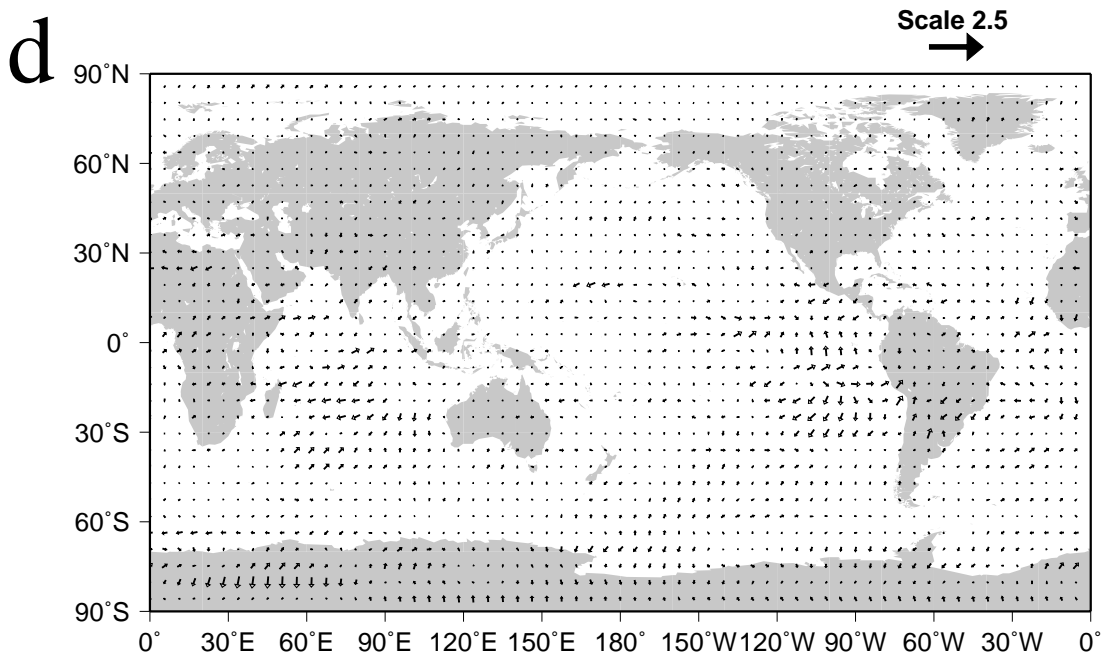
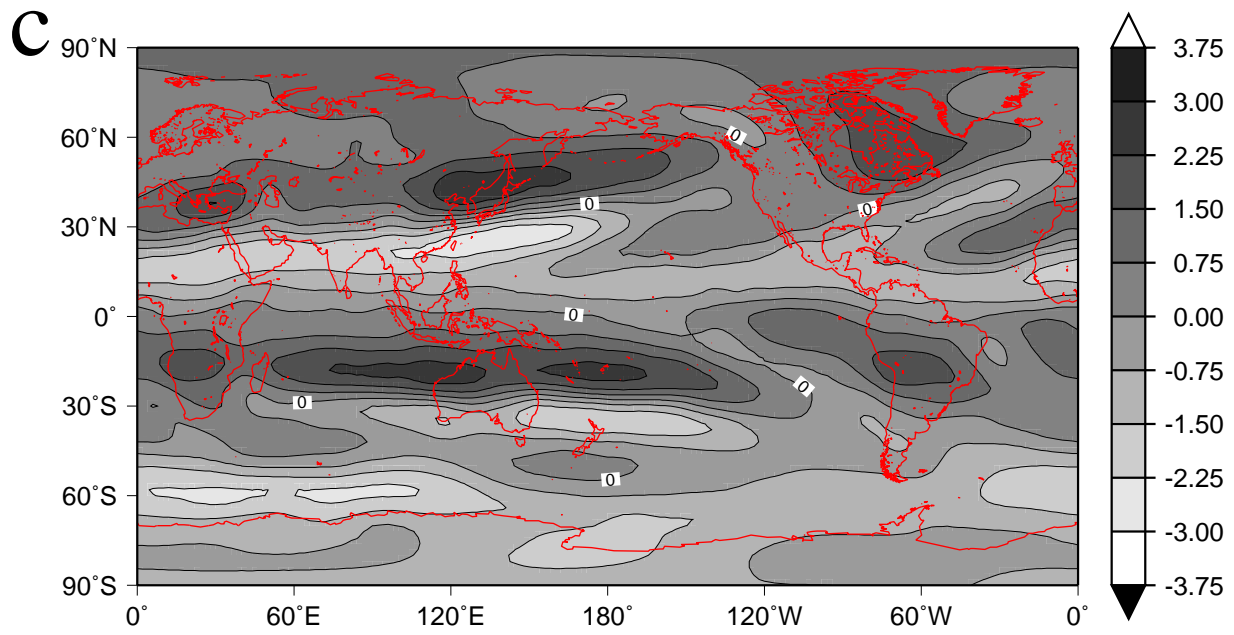


Figure 8. (c) and (d).

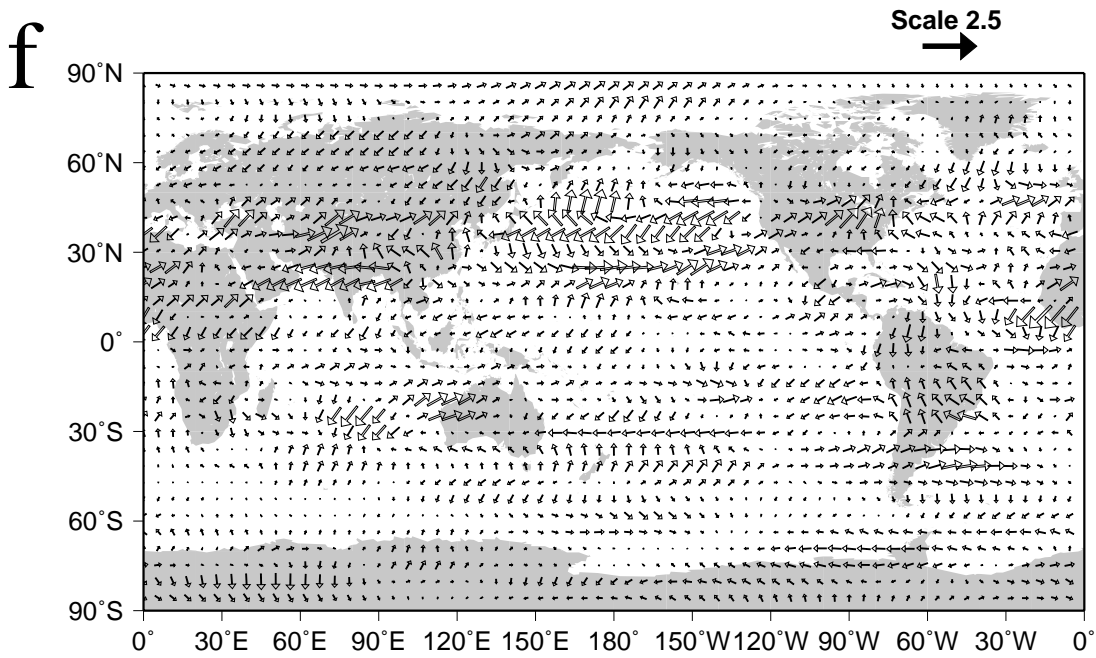
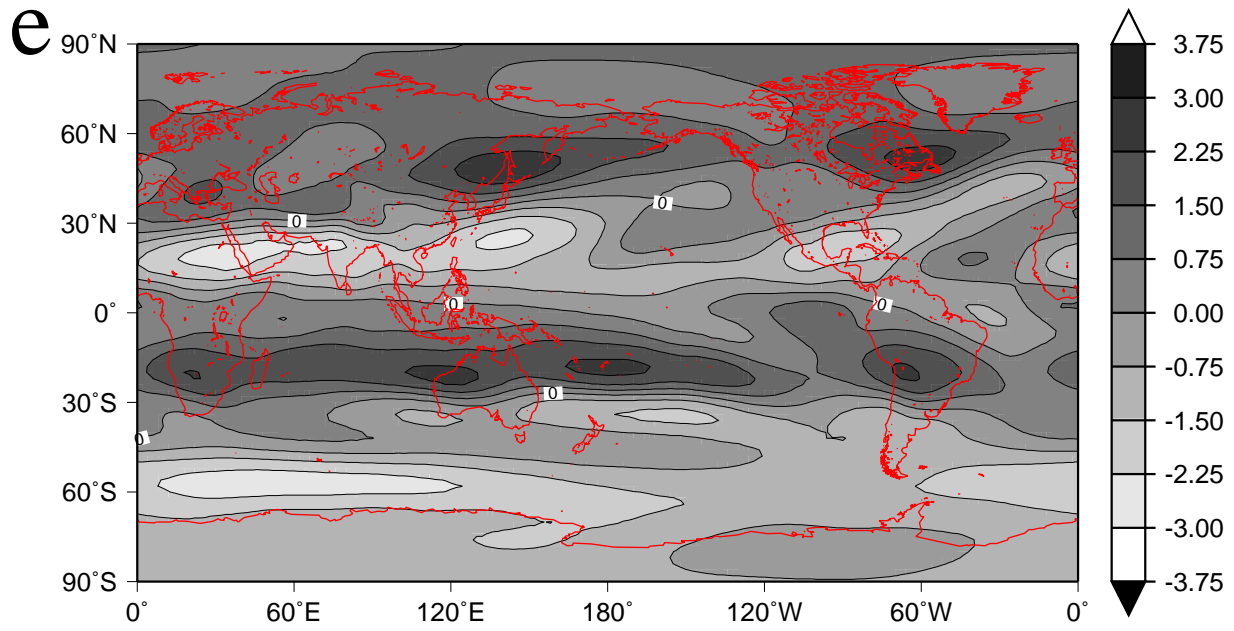


Figure 8. (e) and (f).

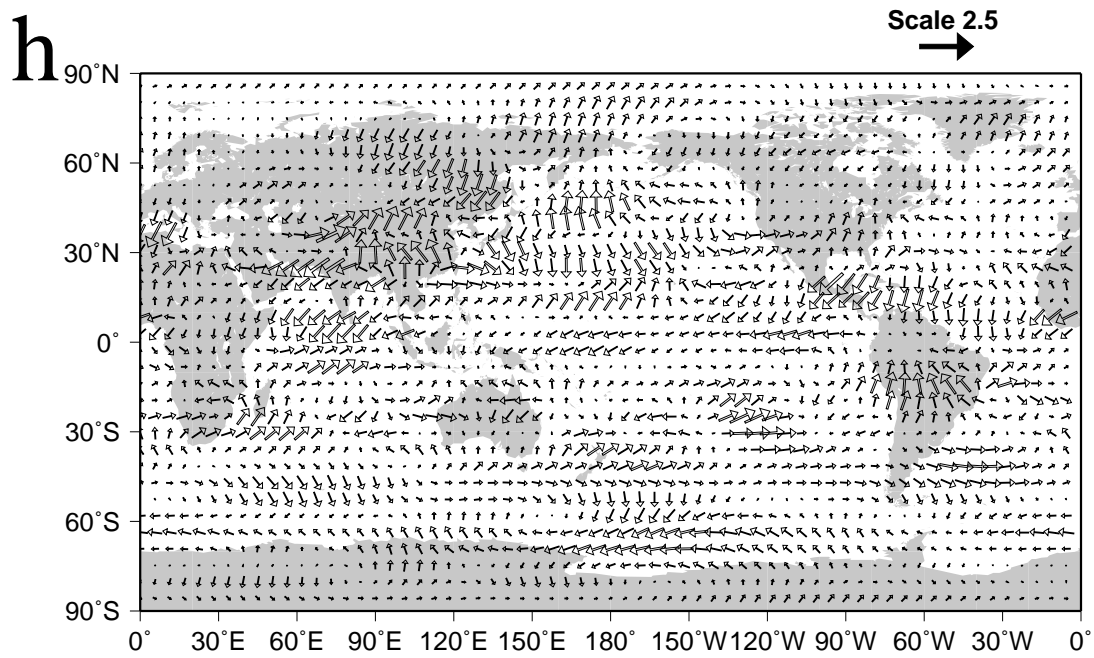
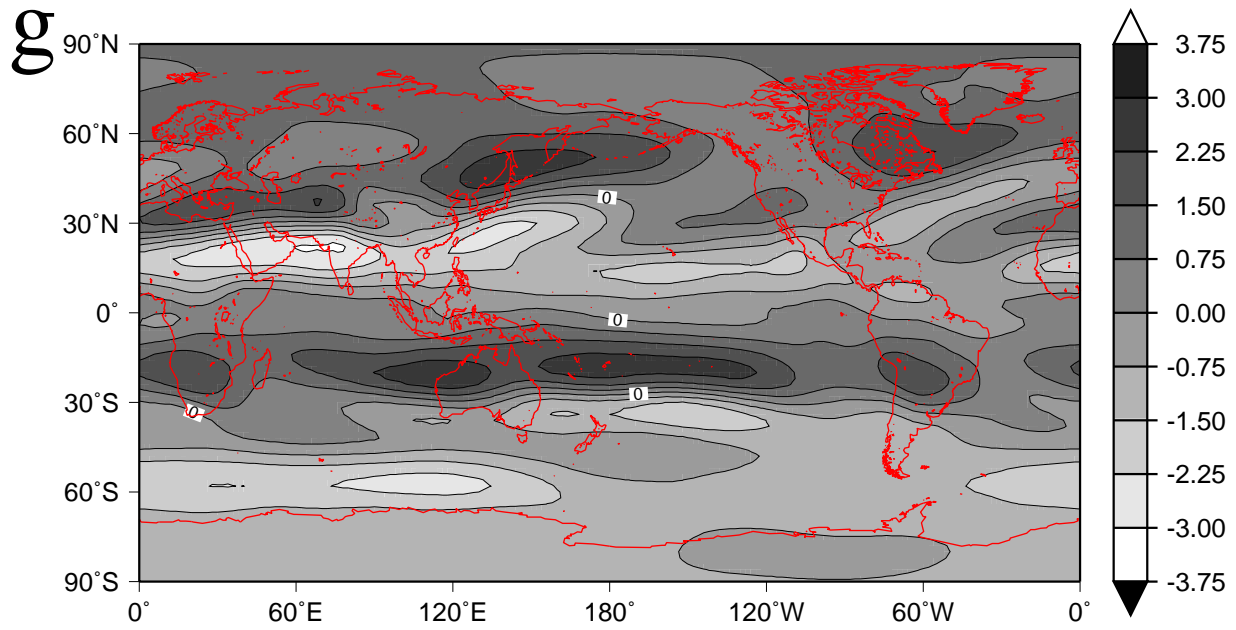


Figure 8. (g) and (h).

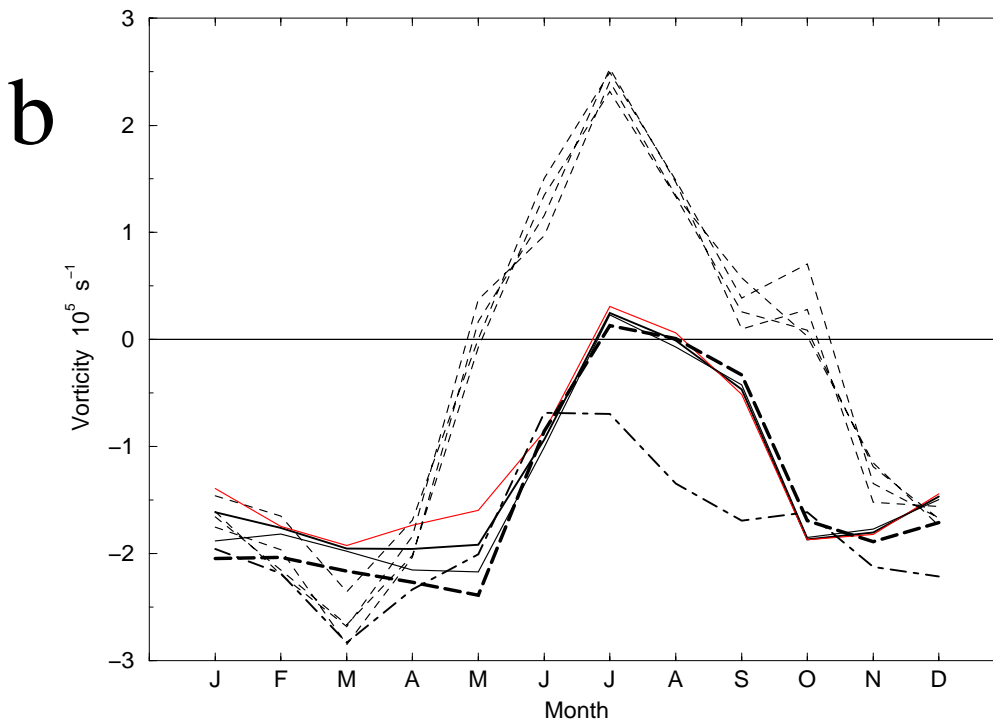
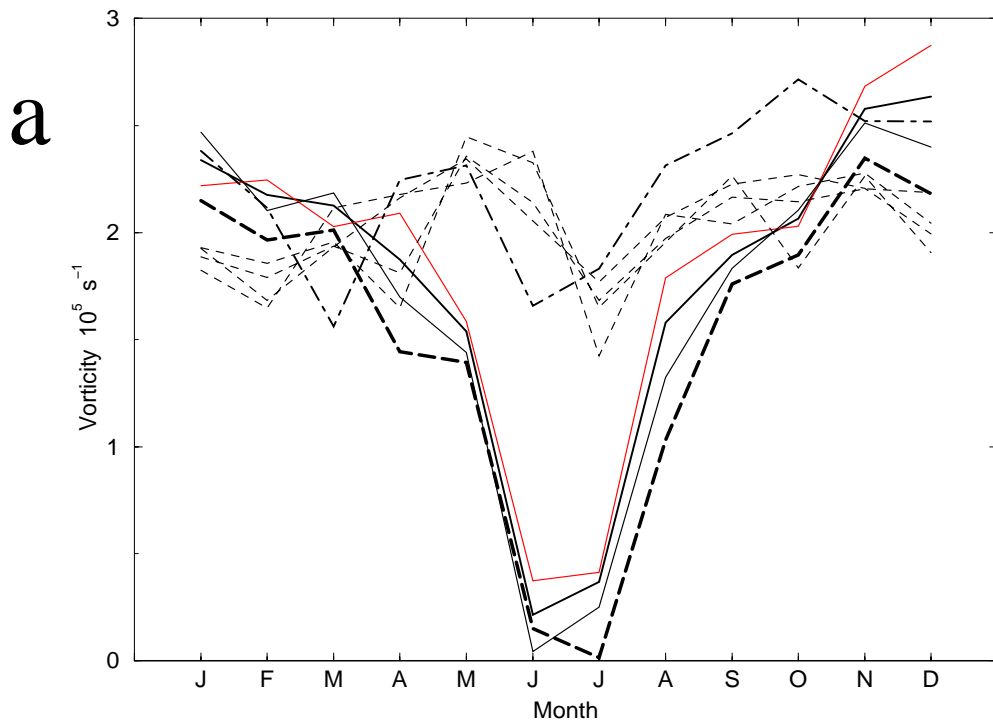


Figure 9. (a) and (b).

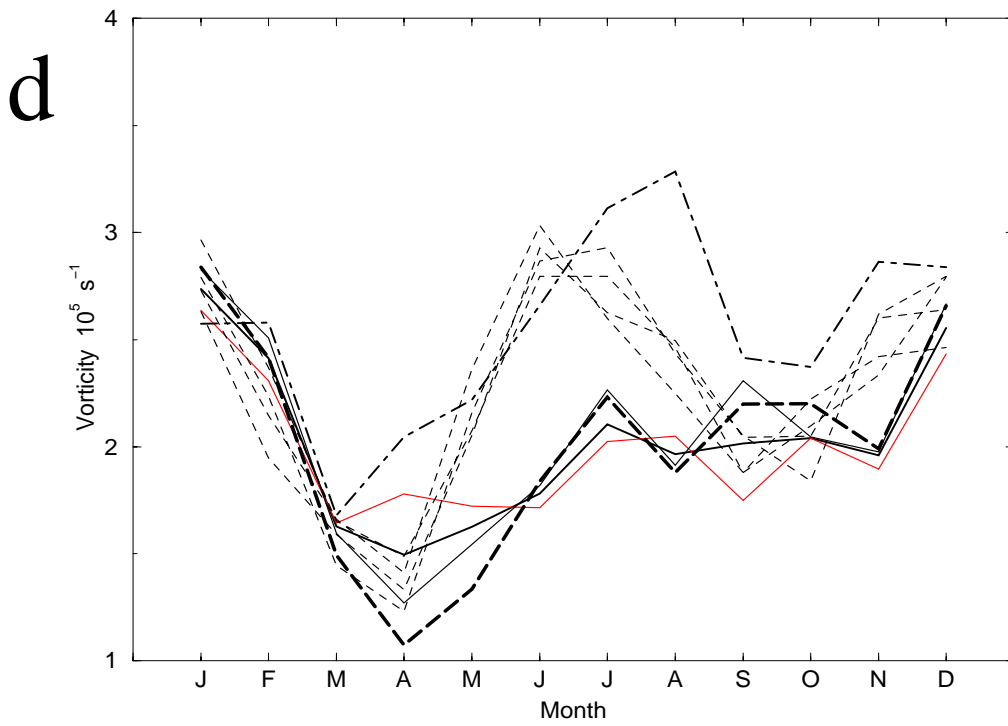
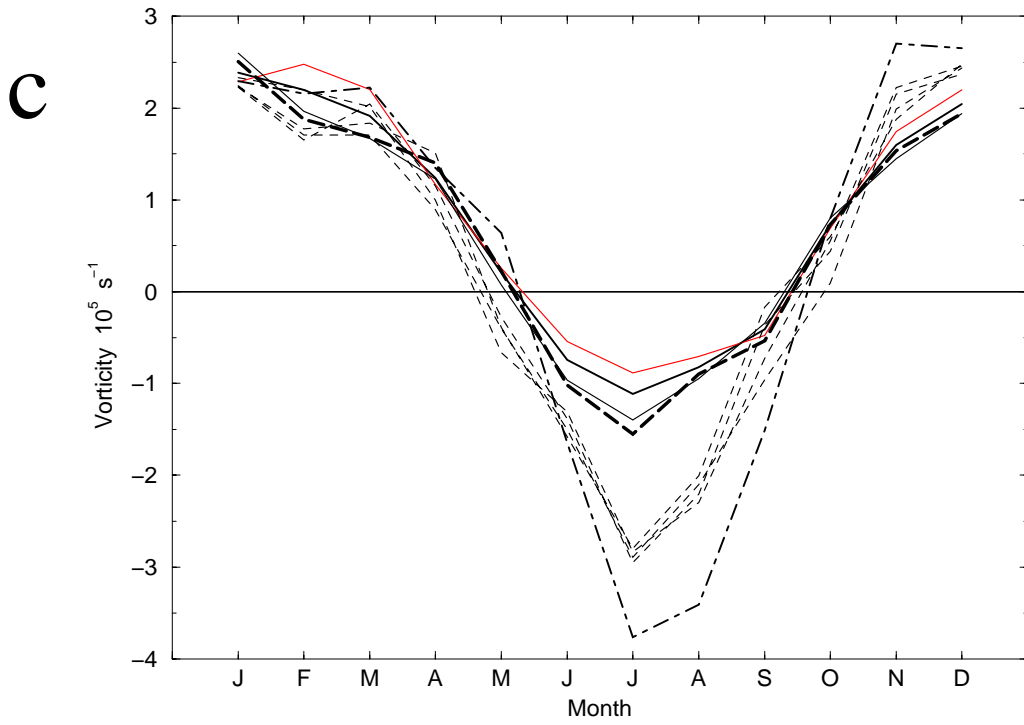


Figure 9. (c) and (d).

e

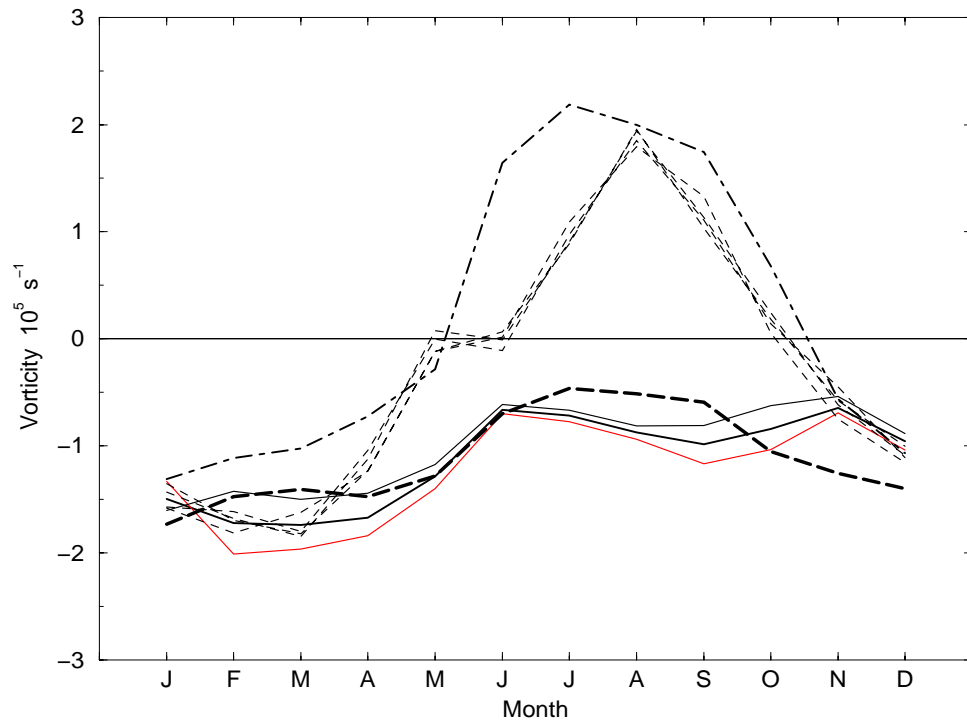


Figure 9. (e).

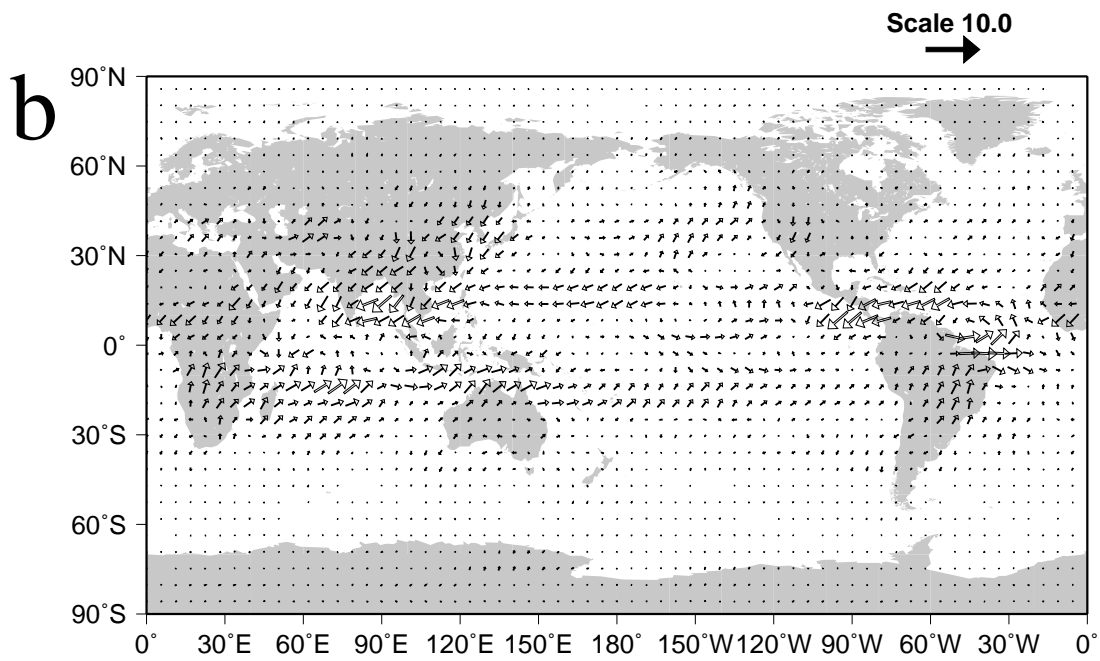
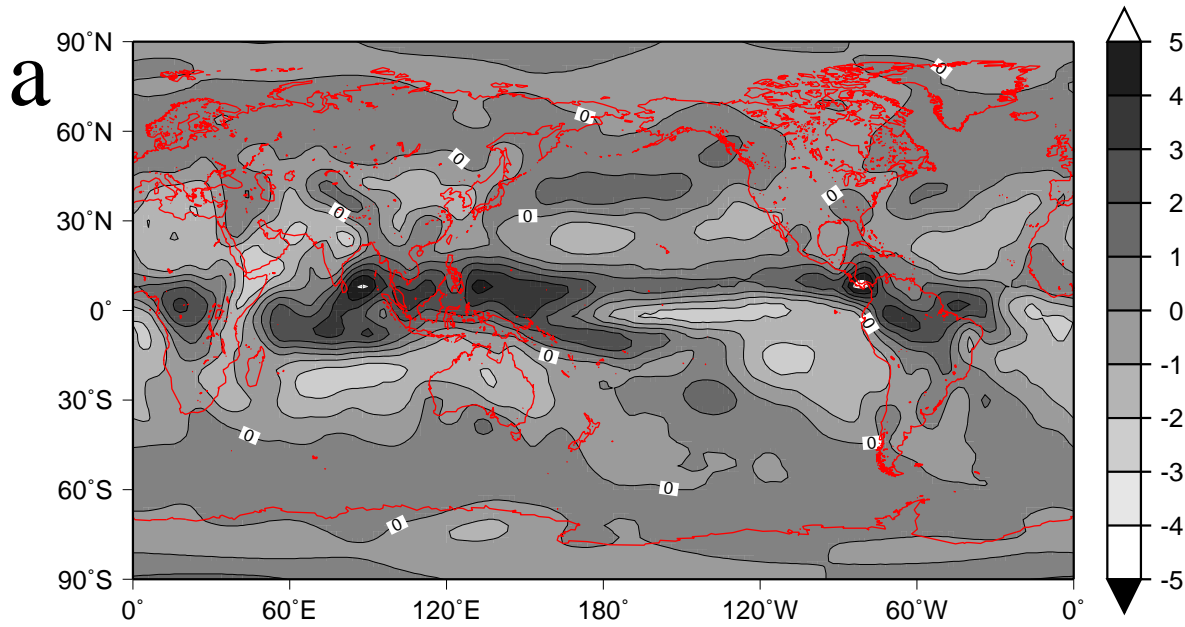


Figure 10. (a) and (b).

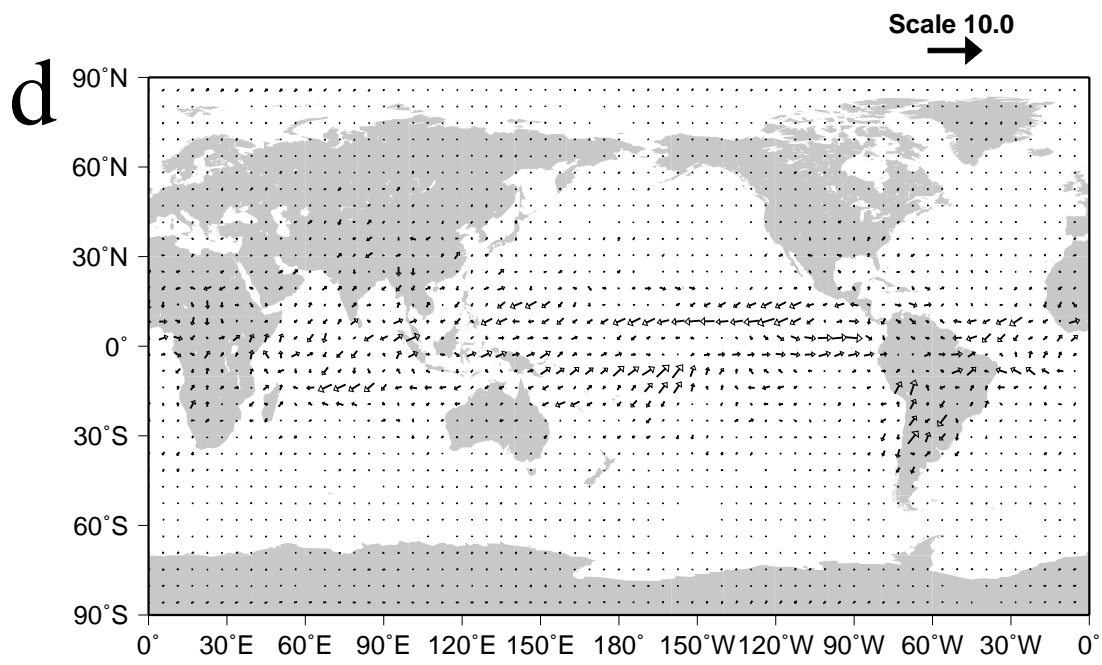
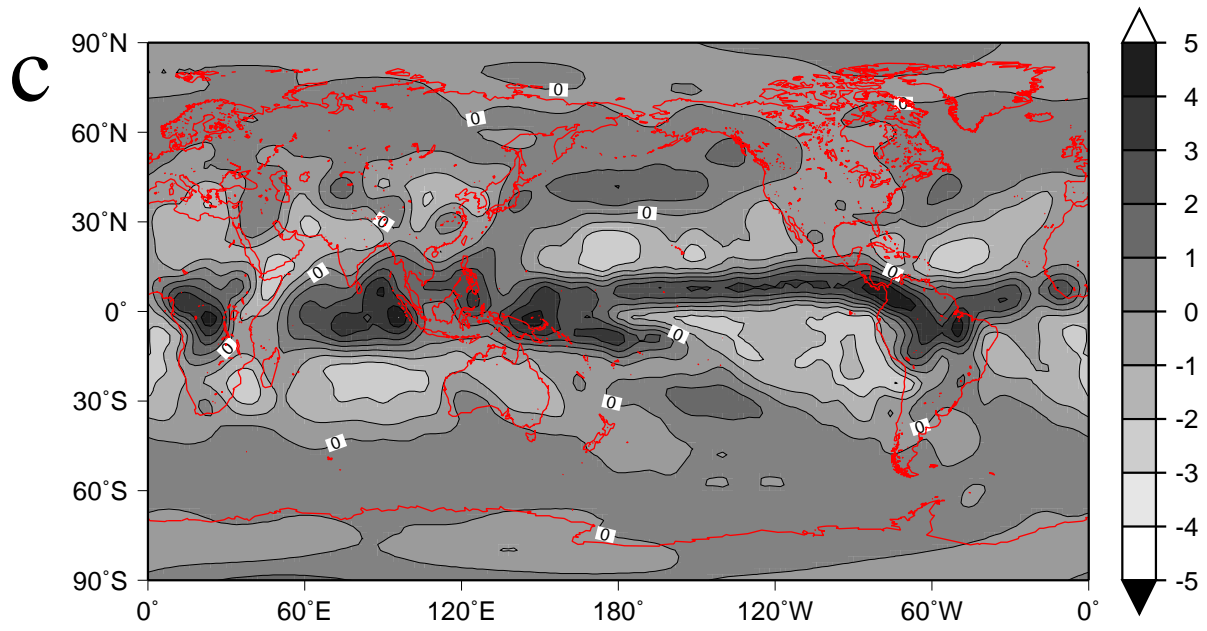


Figure 10. (c) and (d).

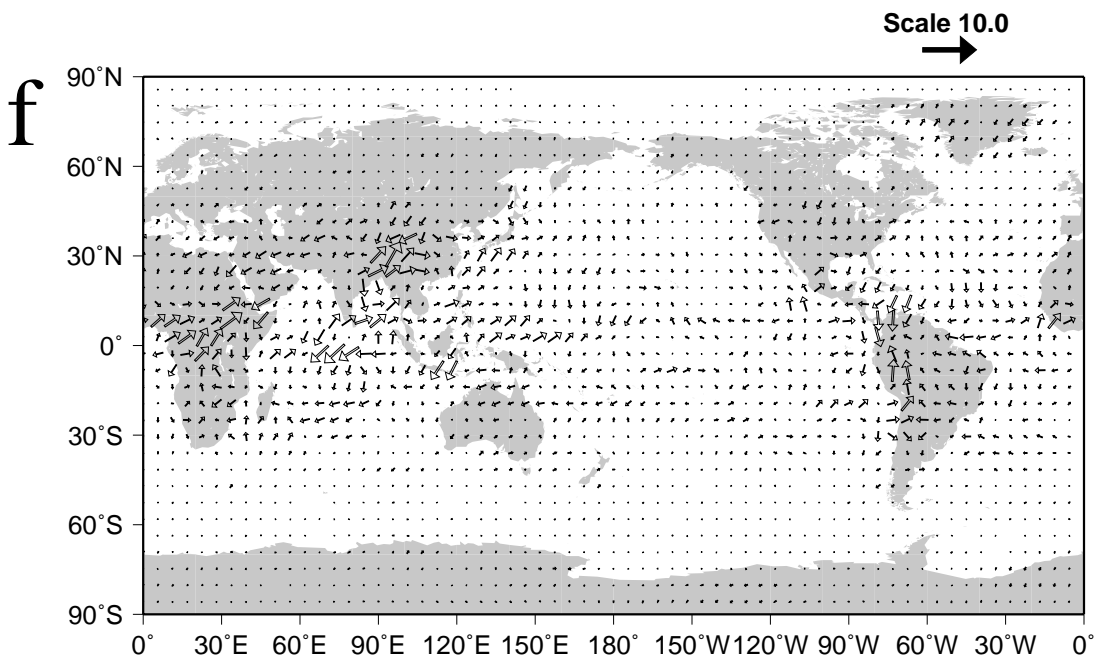
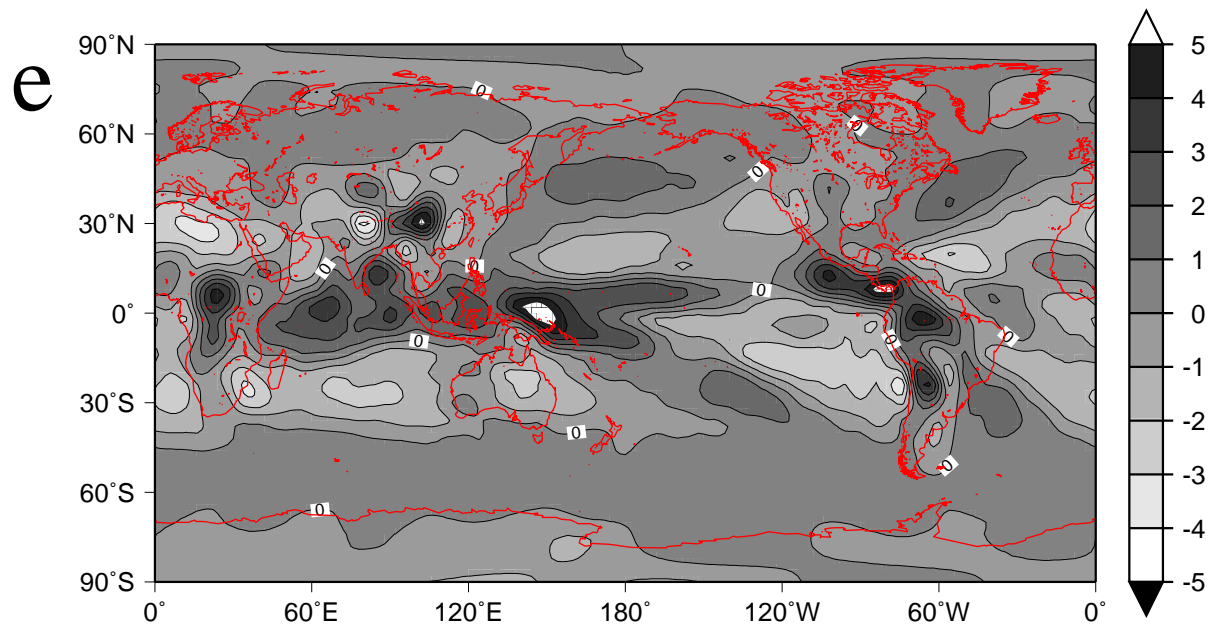


Figure 10. (e) and (f).

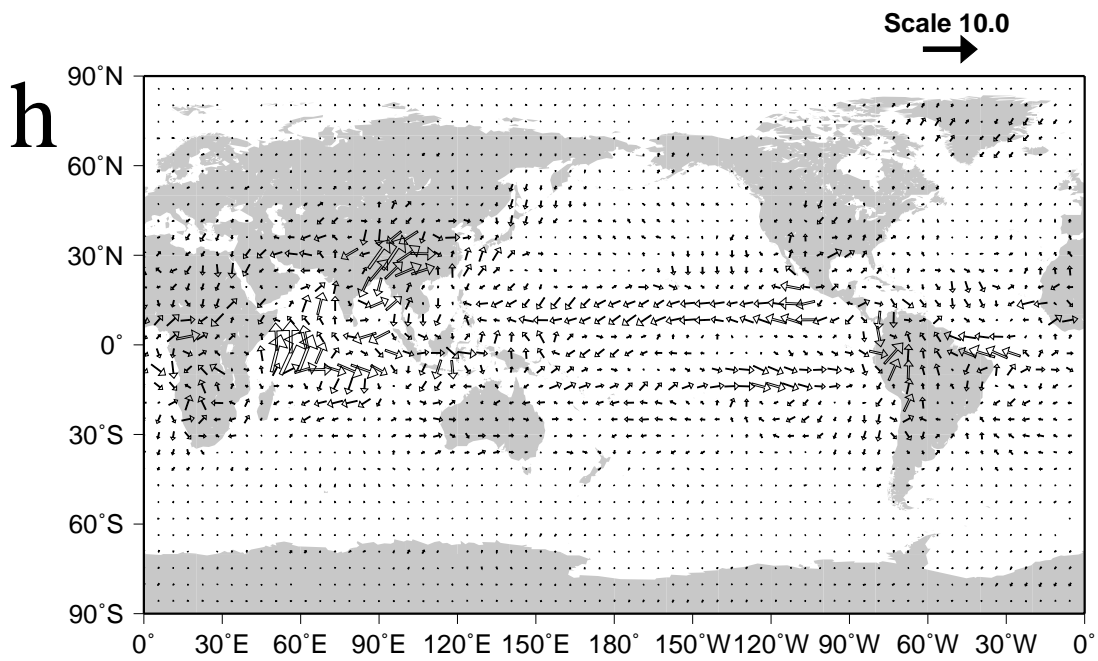
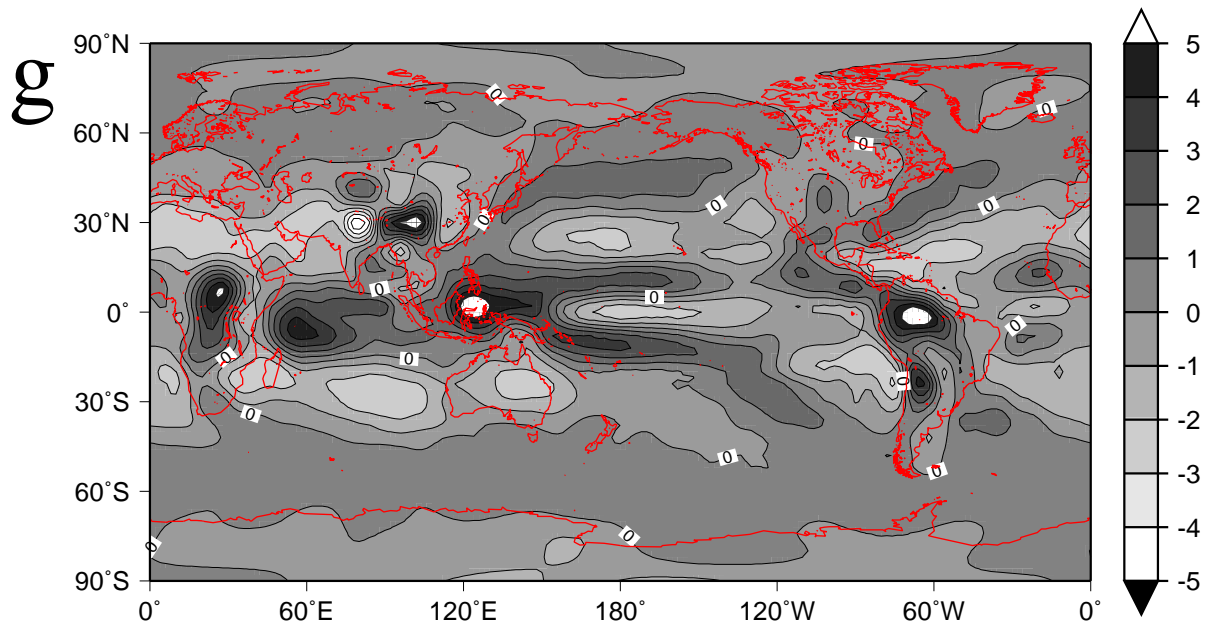


Figure 10. (g) and (h).

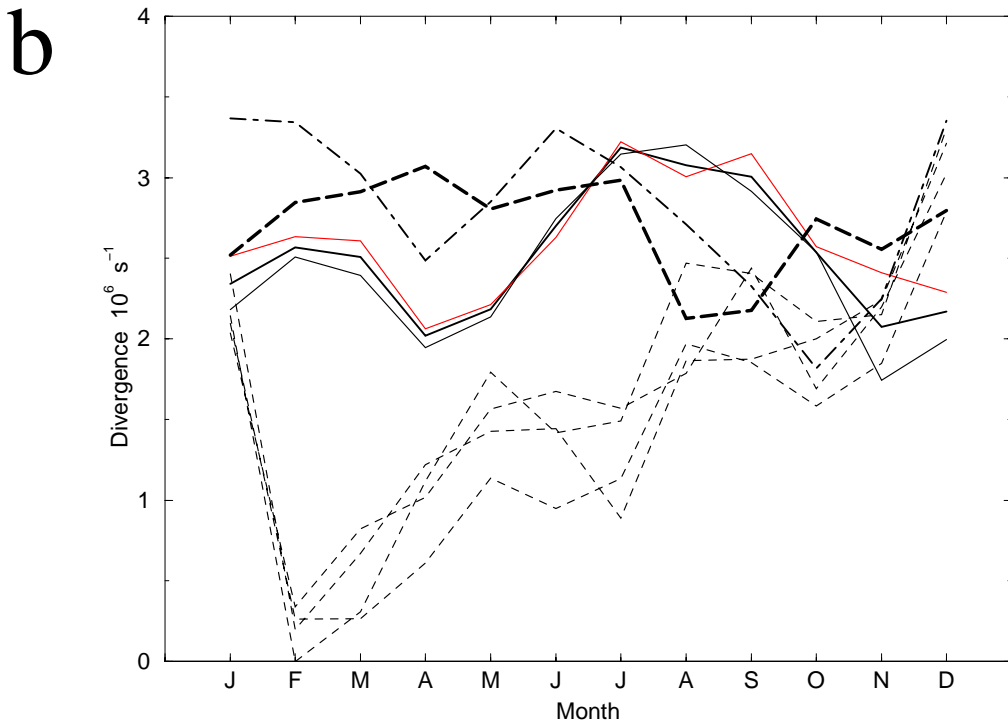
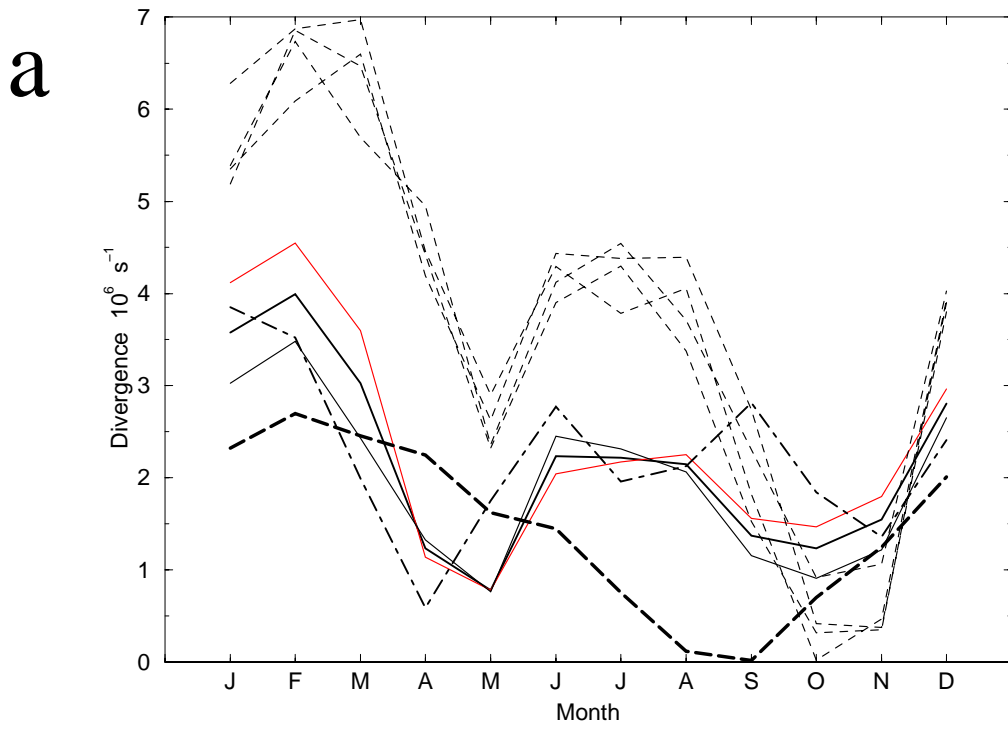


Figure 11. (a) and (b).

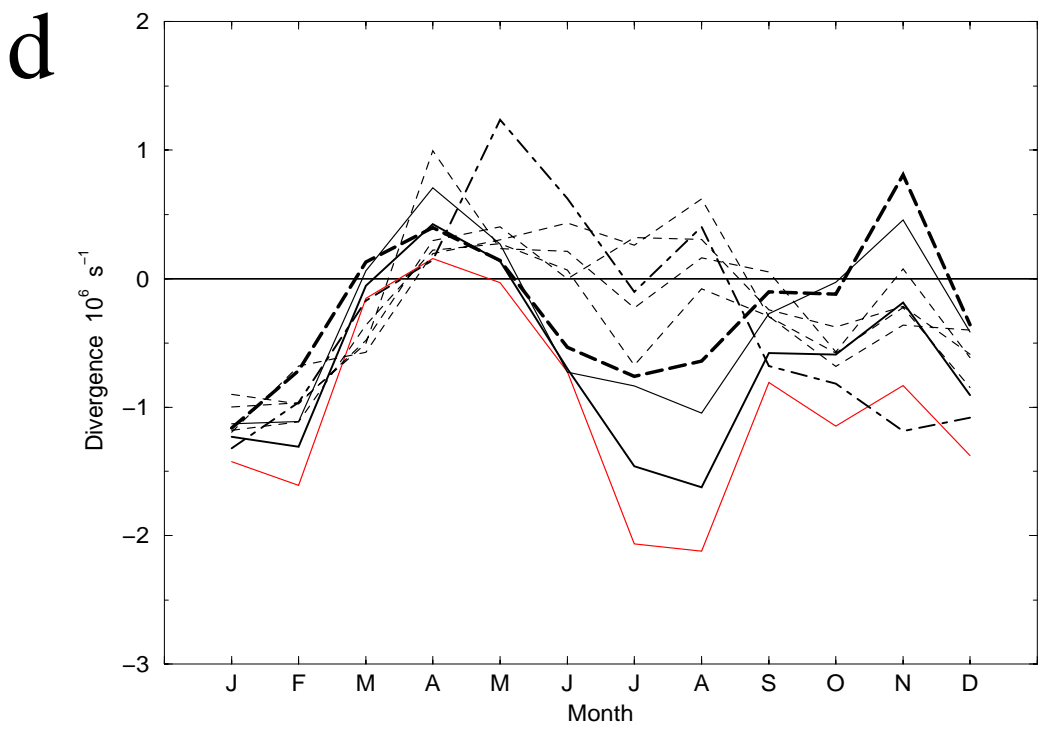
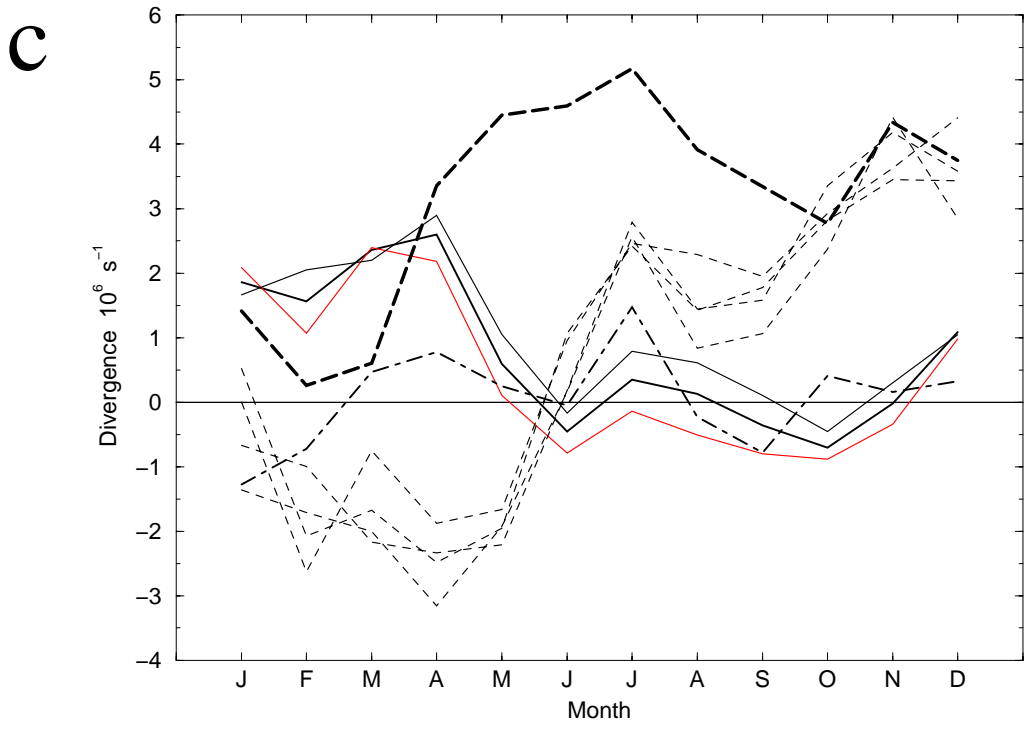


Figure 11. (c) and (d).

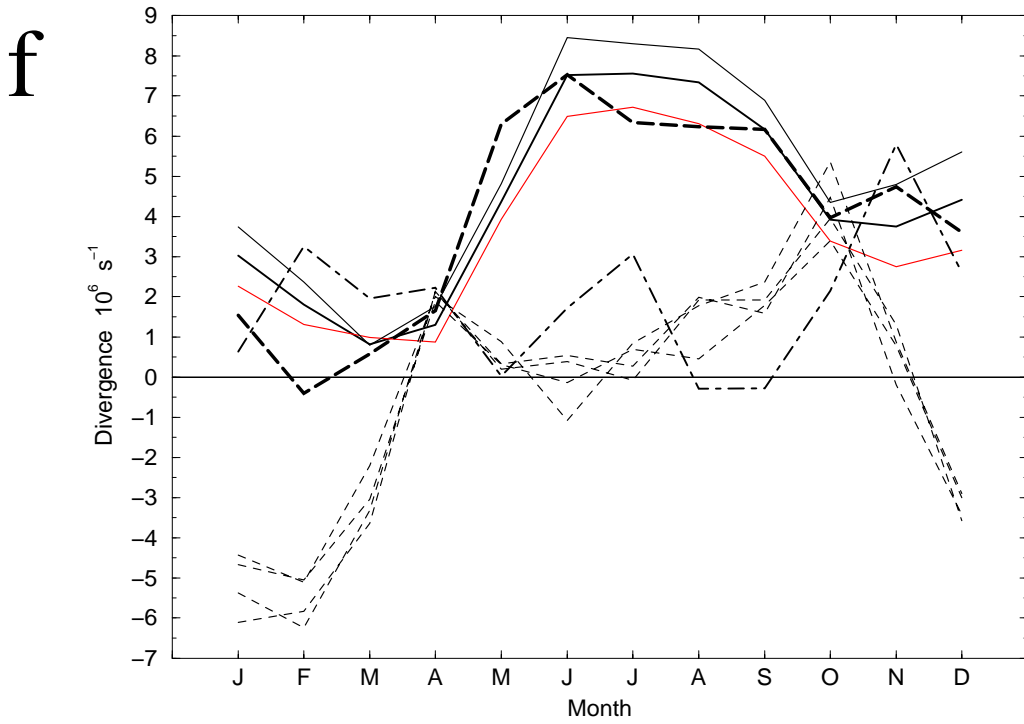
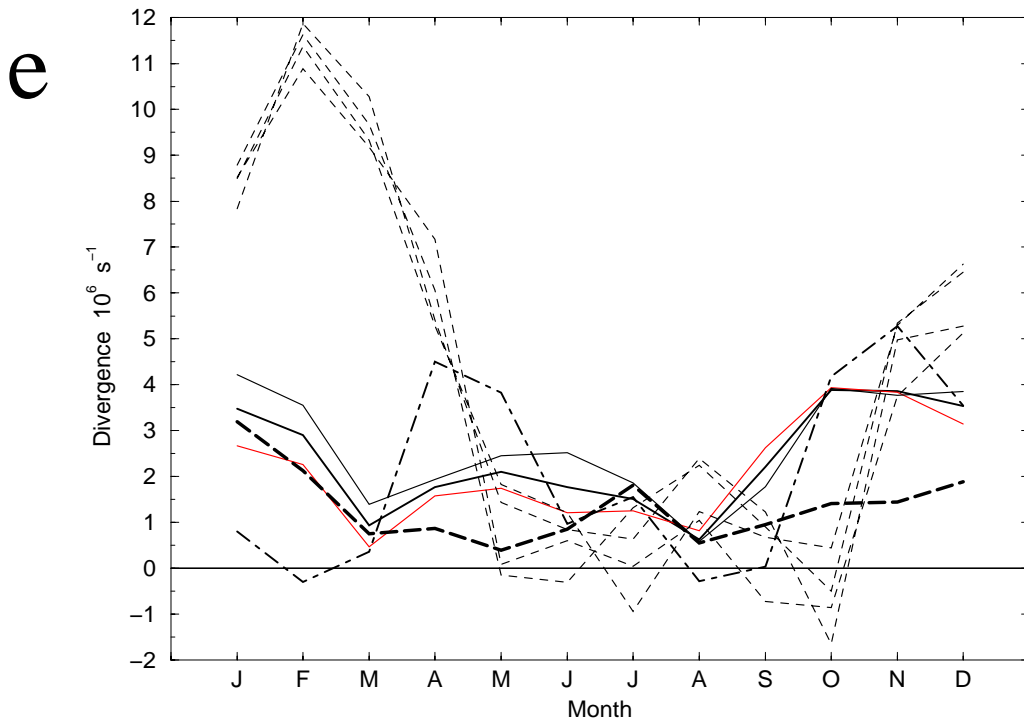


Figure 11. (e) and (f).

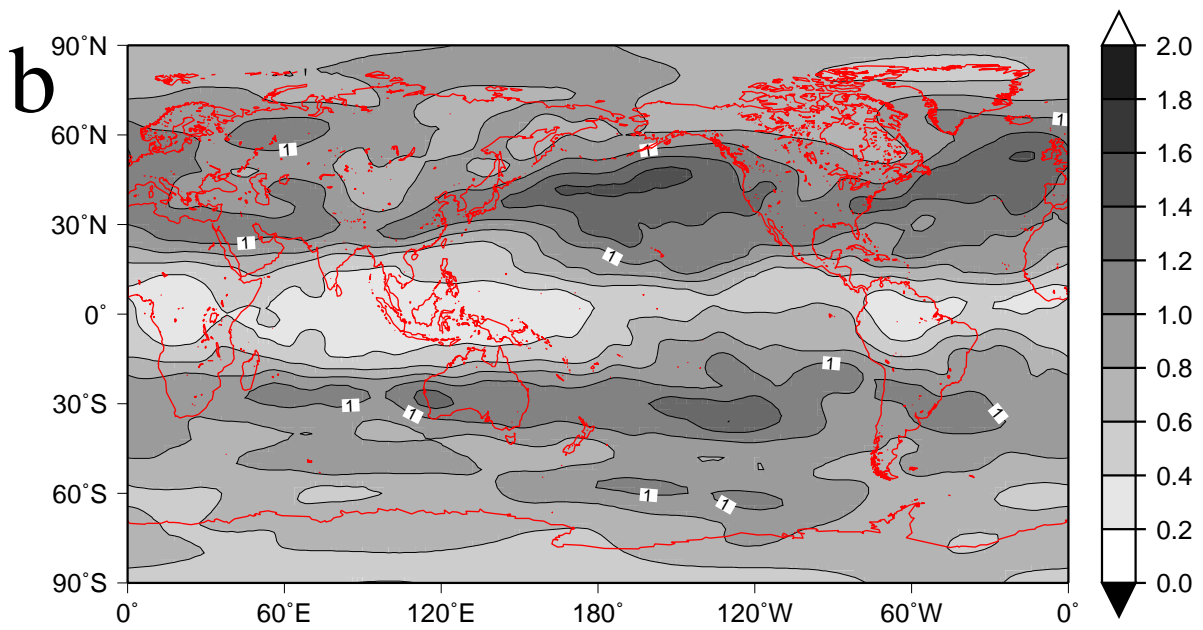
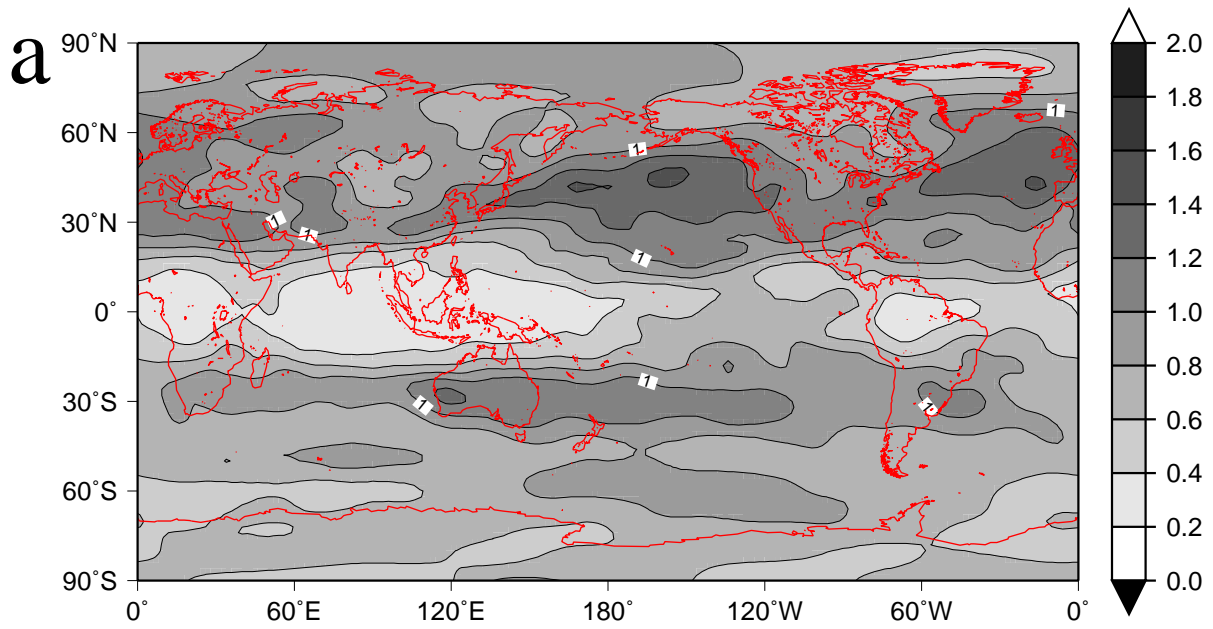


Figure 12. (a) and (b).

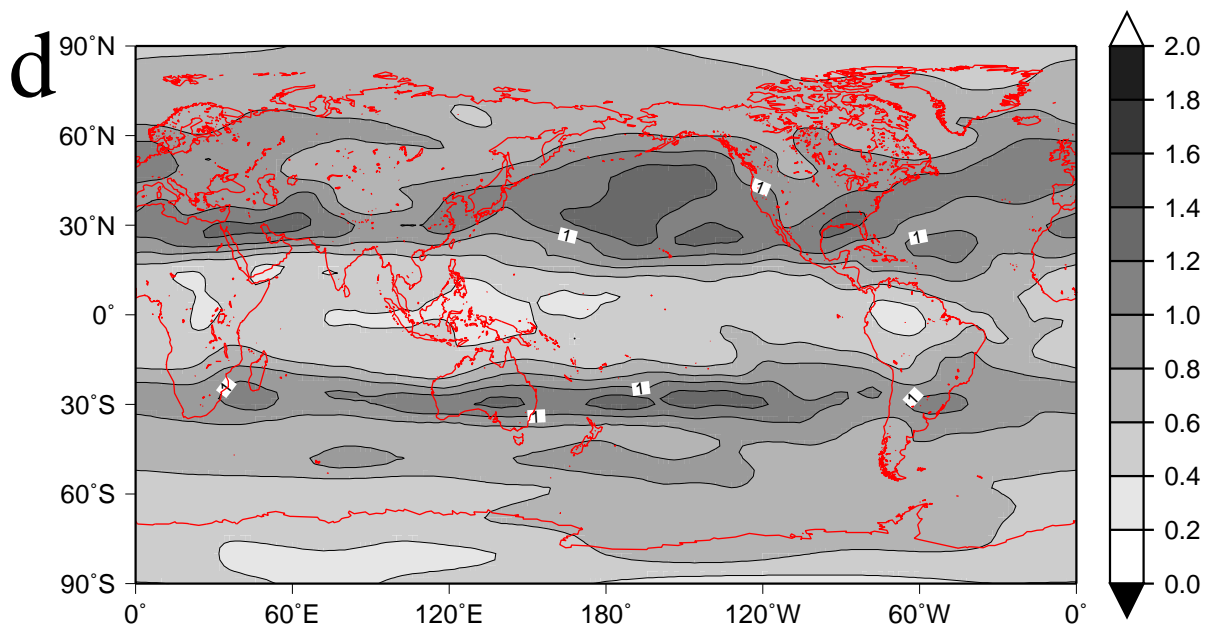
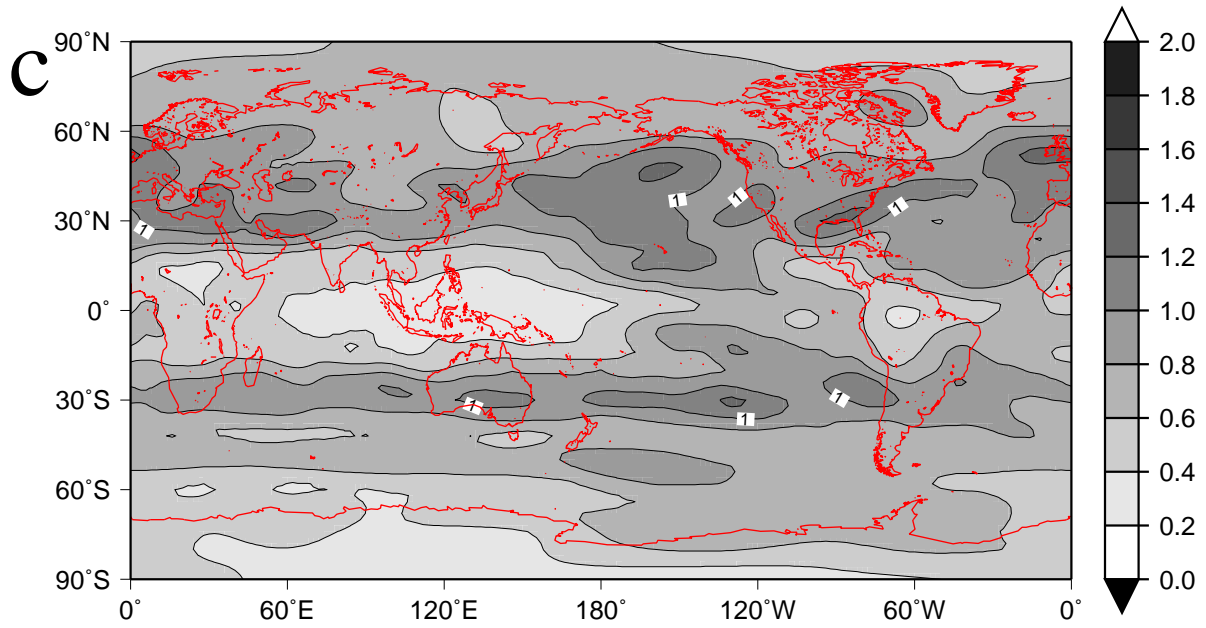


Figure 12. (c) and (d).

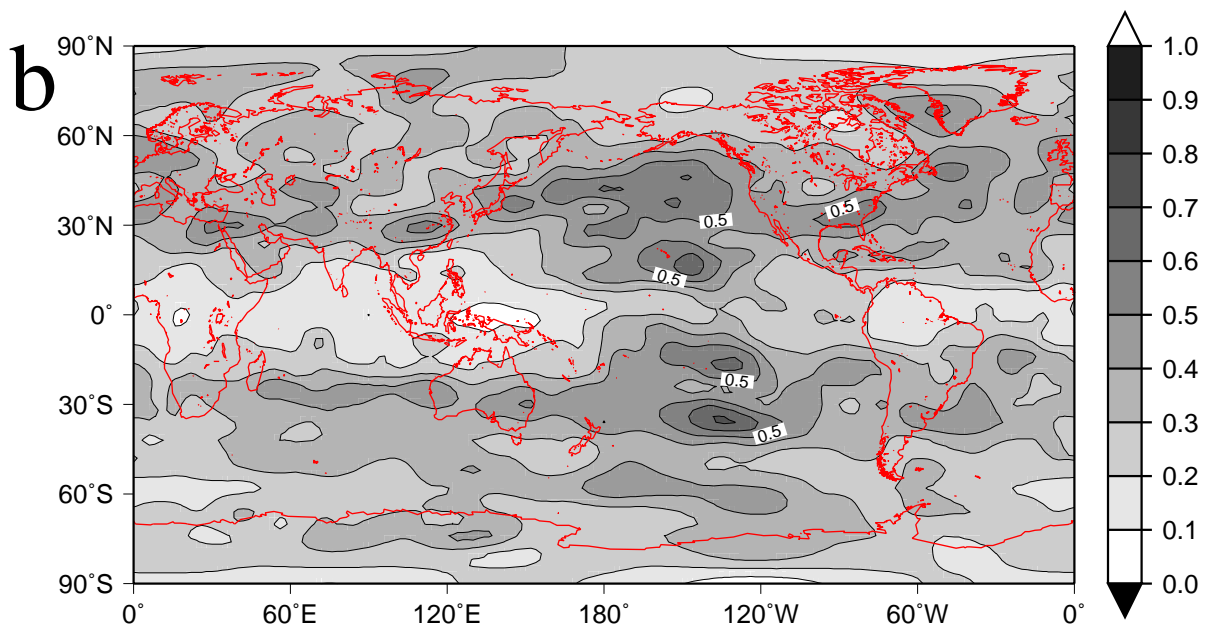
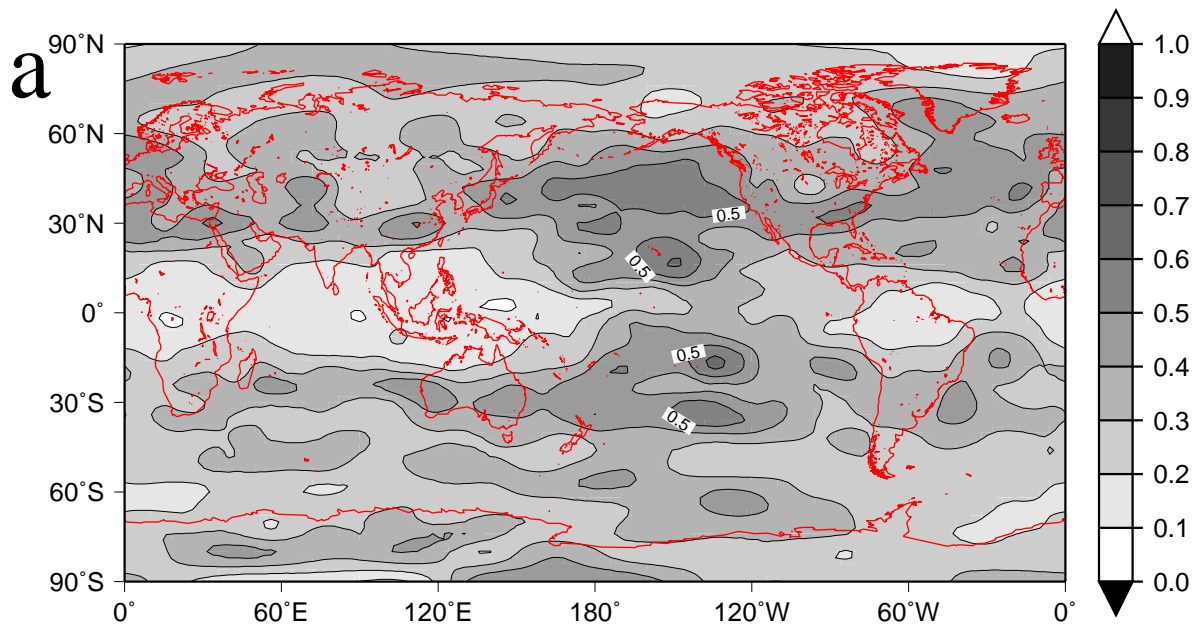


Figure 13. (a) and (b).

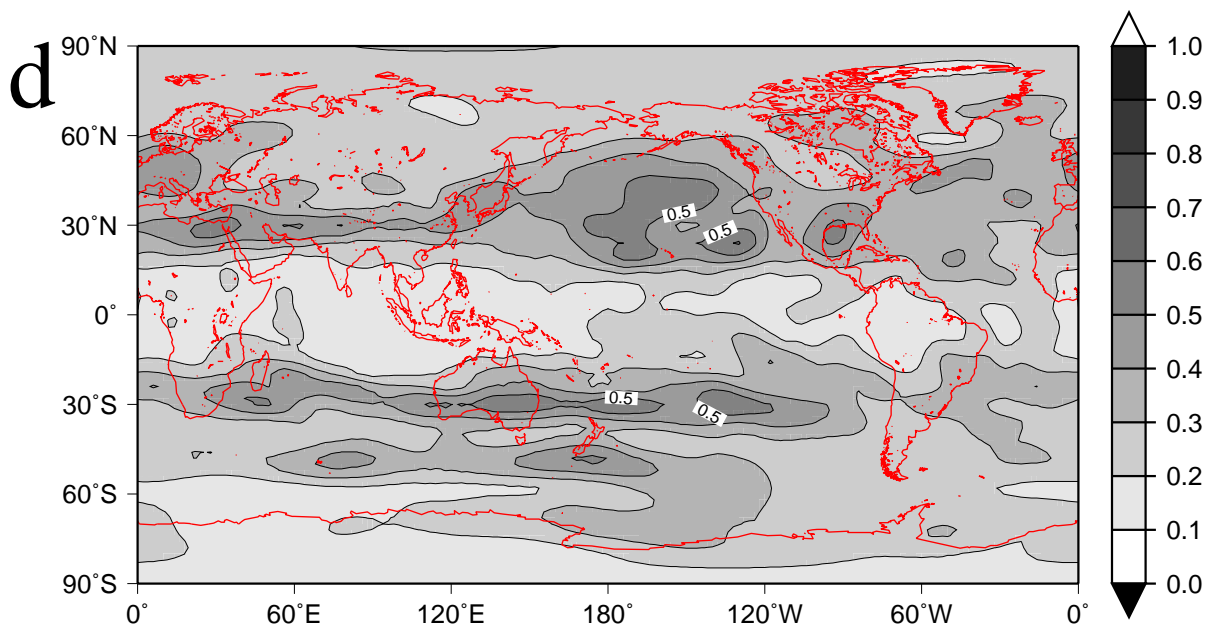
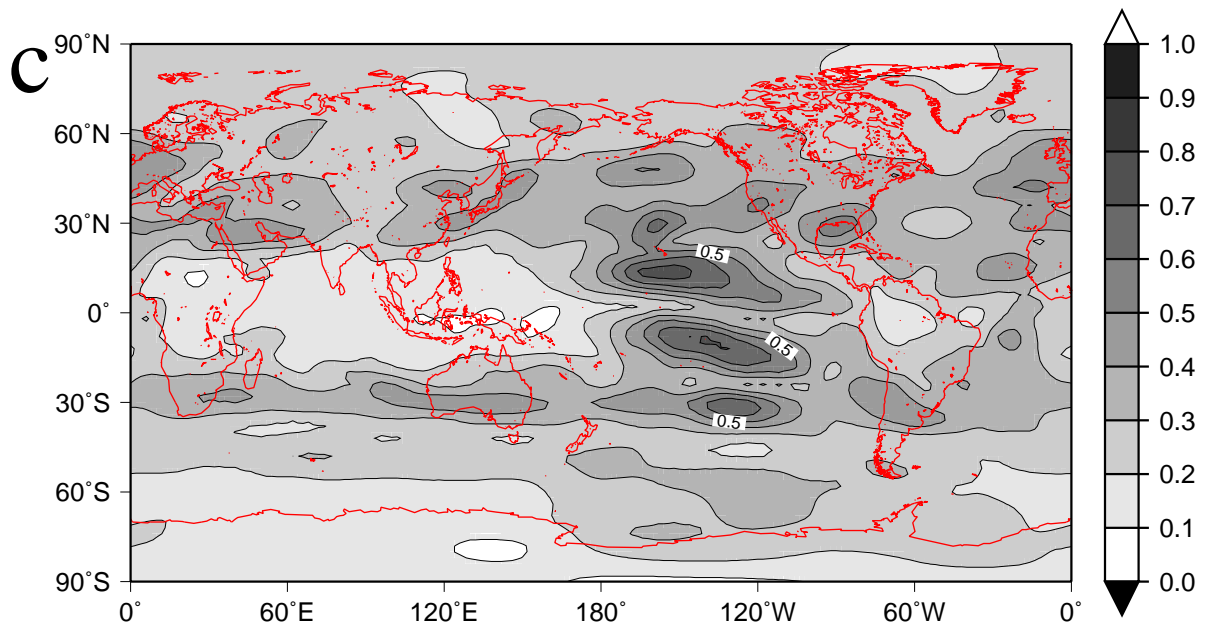


Figure 13. (c) and (d).

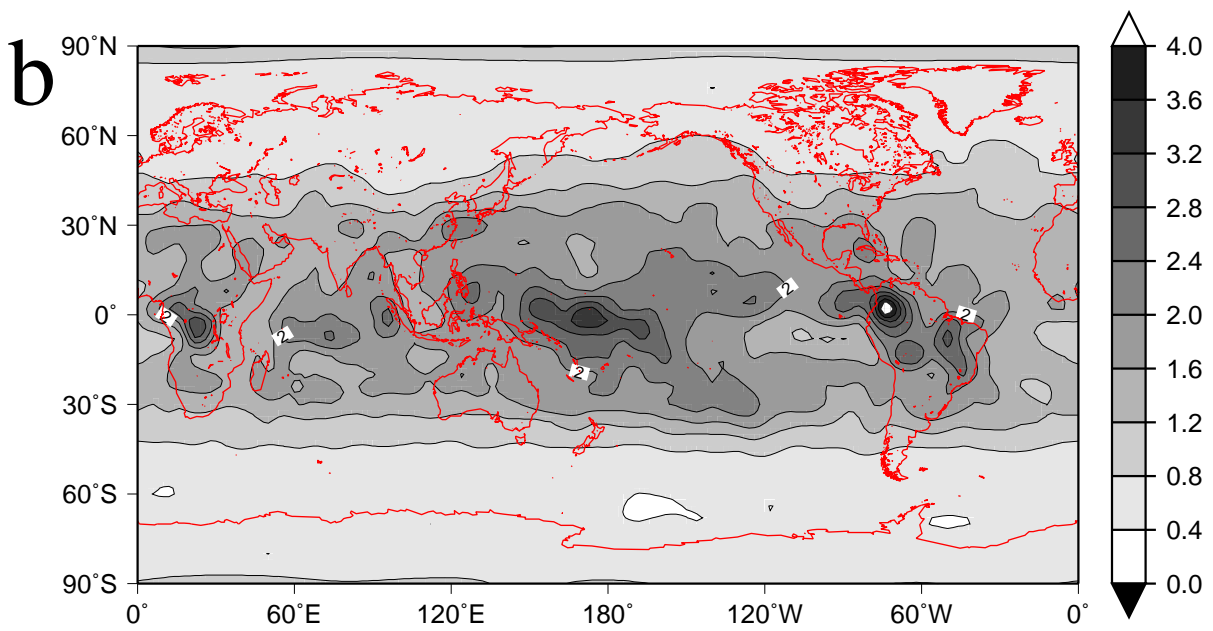
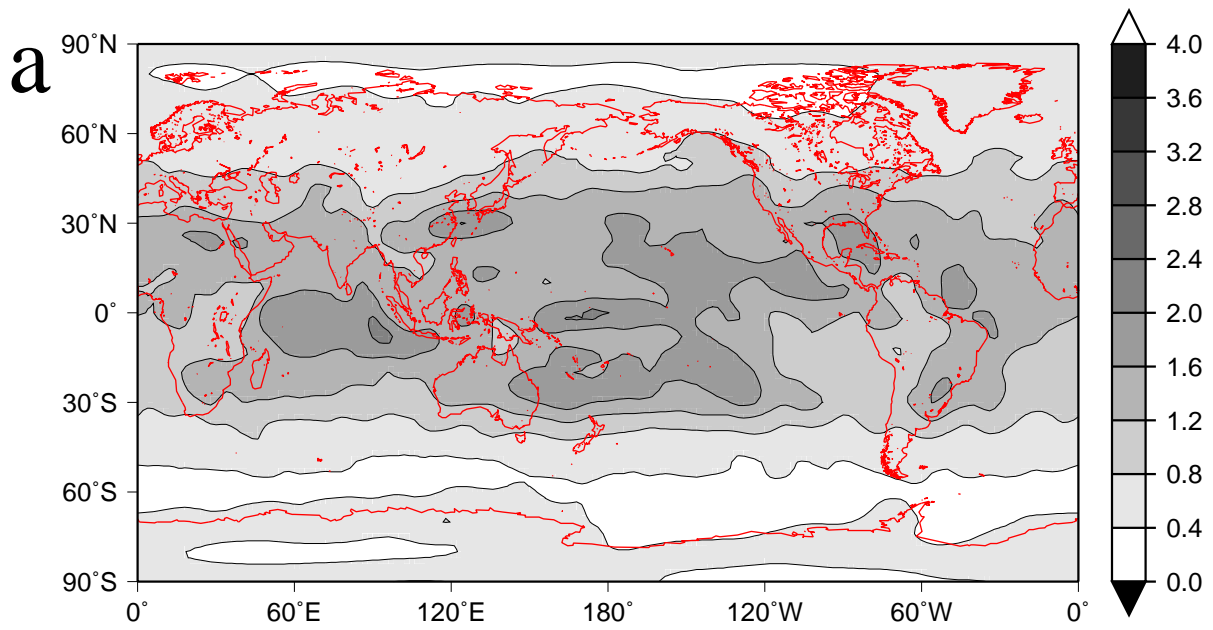


Figure 14. (a) and (b).

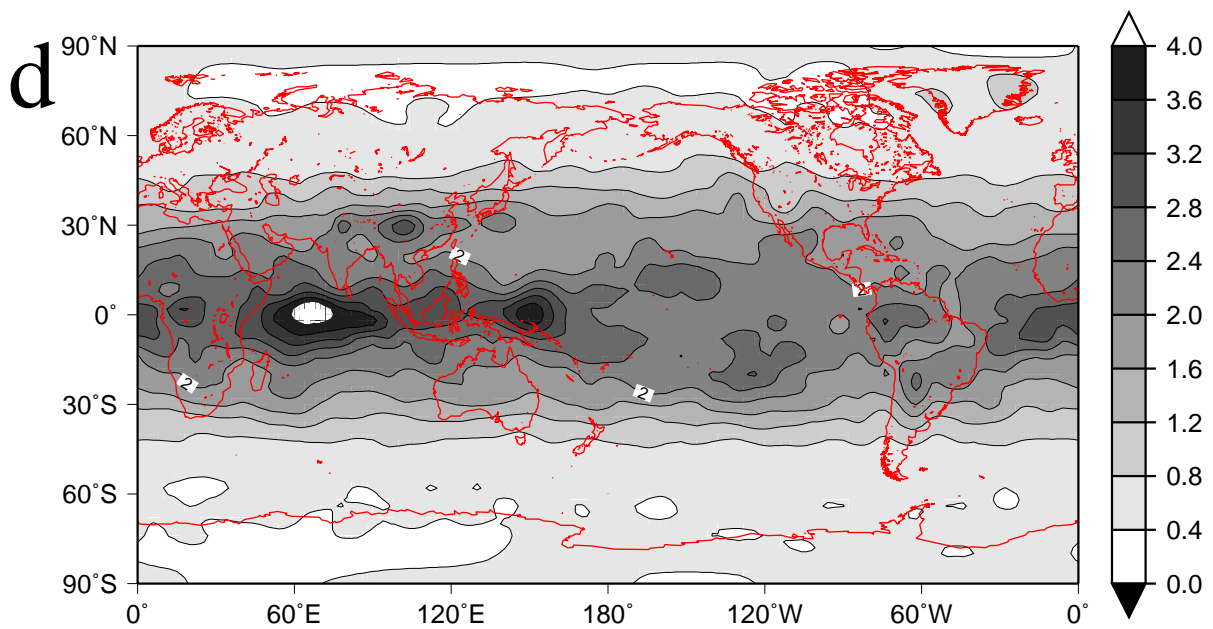
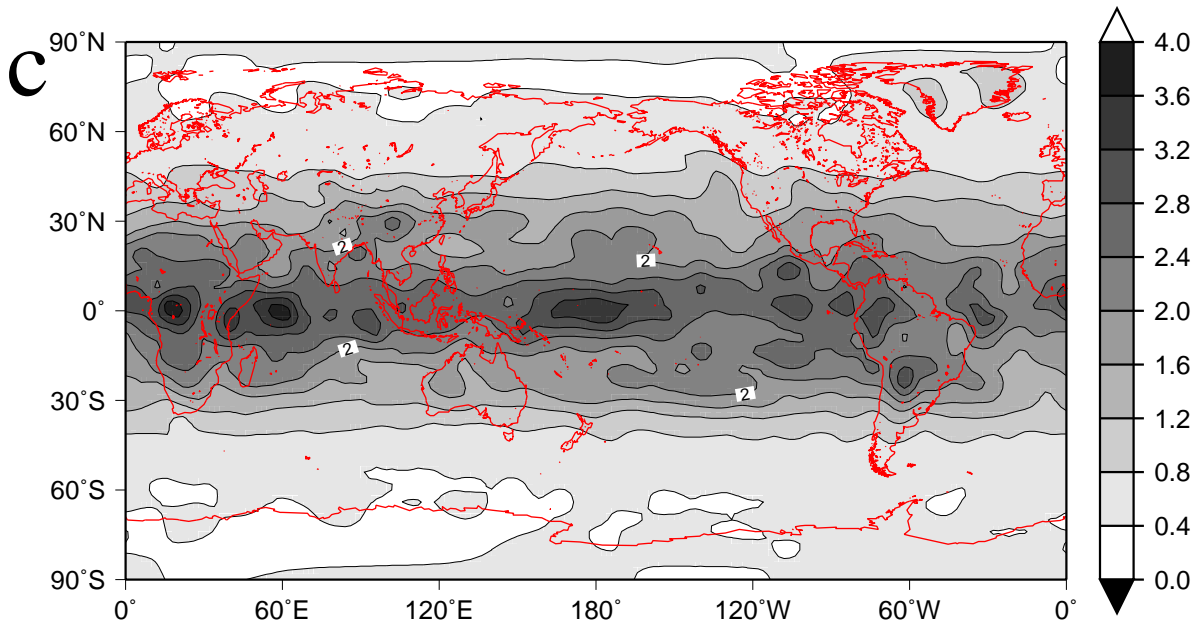


Figure 14. (c) and (d).

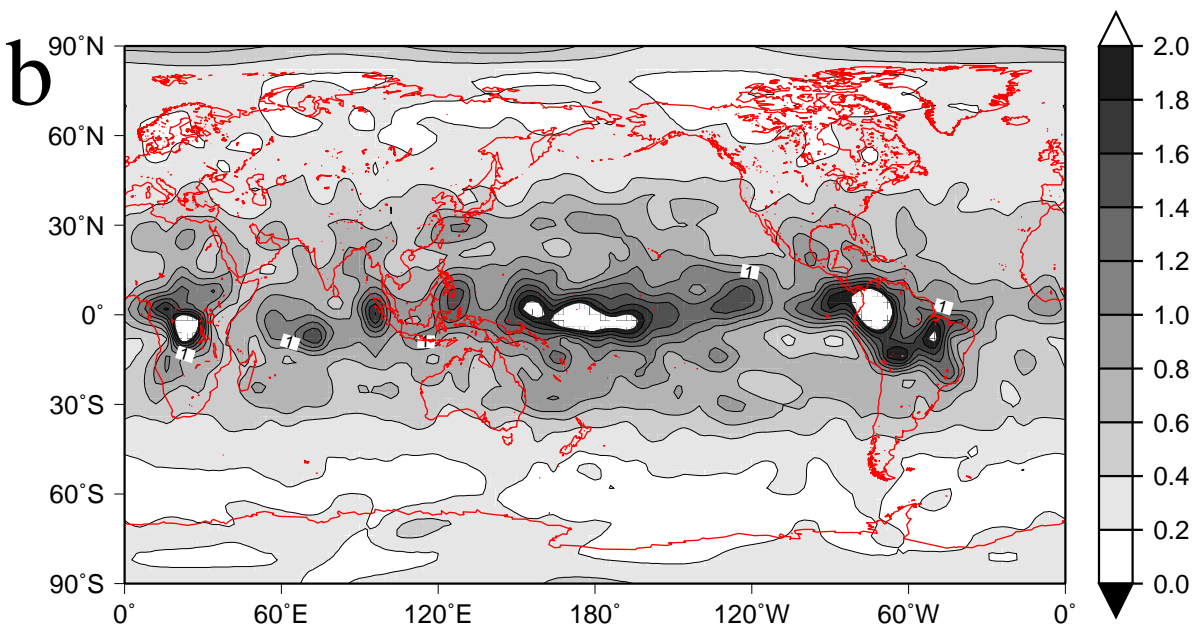
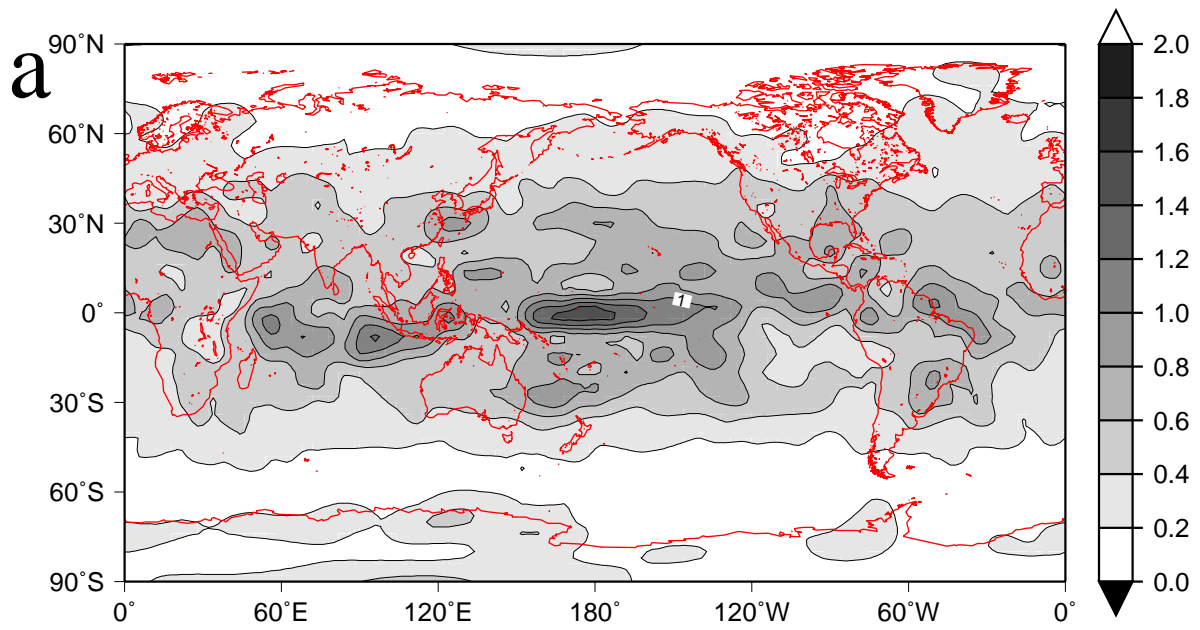


Figure 15. (a) and (b).

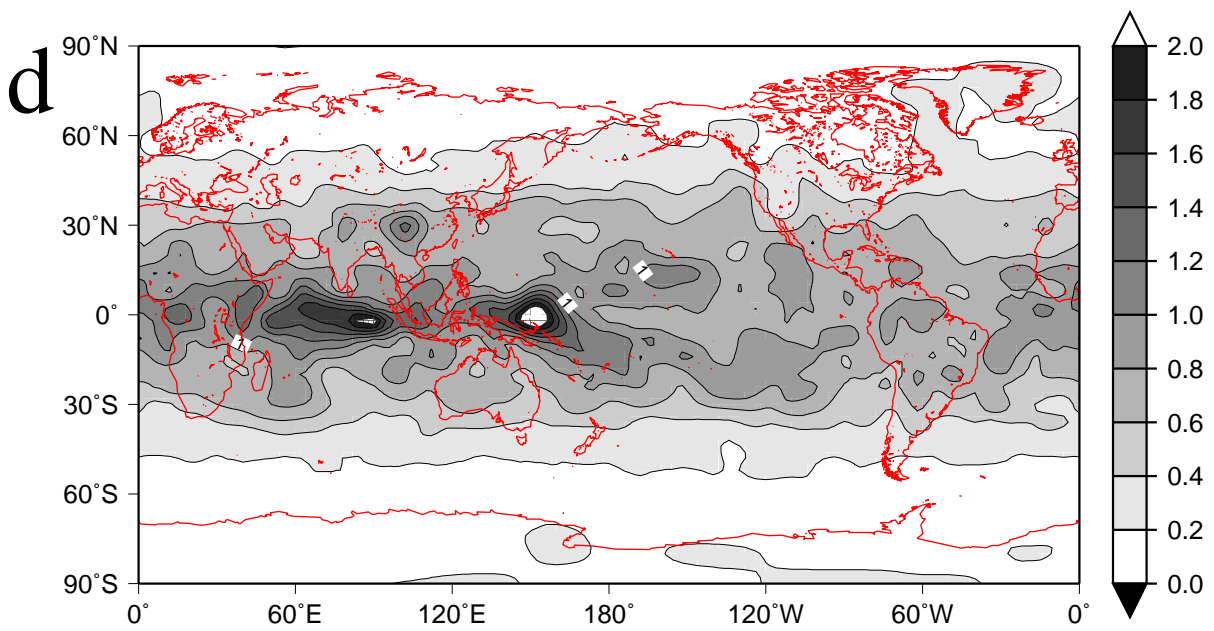
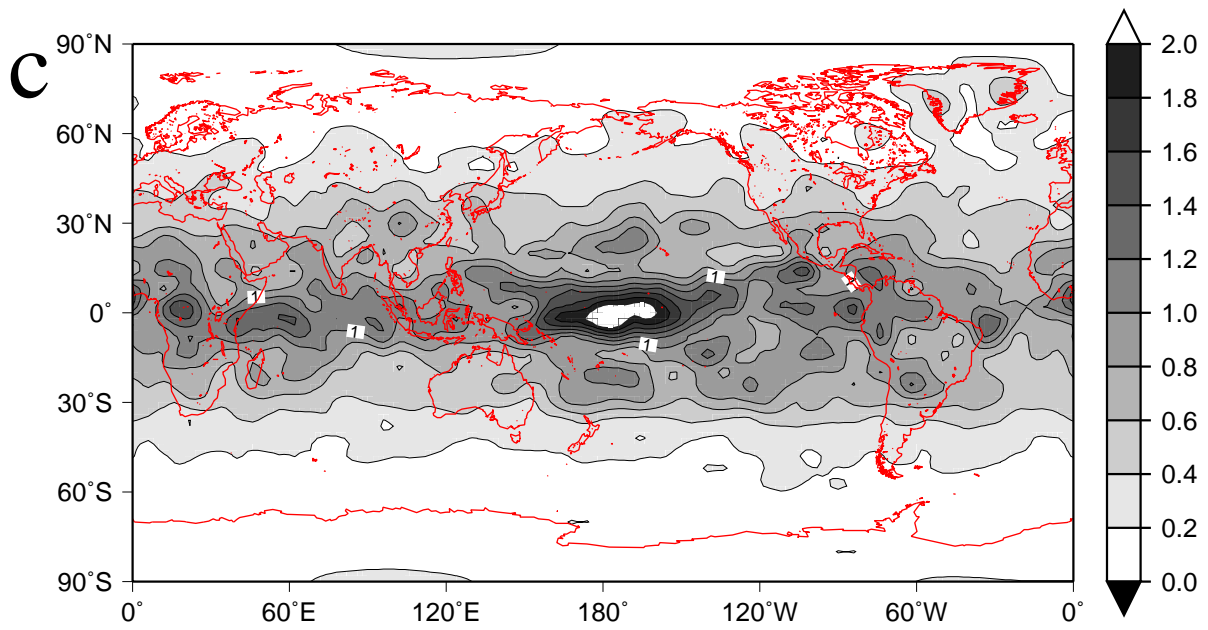


Figure 15. (c) and (d).

Figure Captions

Figure 1. (a) Longitude-Time plot of the NCEP reanalysis 200 hPa monthly mean divergence anomaly from 1958 through 1996 averaged from 5S to 5N. Contour interval is $1 \times 10^{-6} \text{ sec}^{-1}$.

(b) Time series of the monthly Southern Oscillation Index from 1958 to 1998. The data are from the Climate Prediction Center of NCEP.

Figure 2. (a) Longitude-Time plot of the NCEP reanalysis 200 hPa monthly mean divergence anomaly from 1979 through 1993 averaged from 5S to 5N. Contour interval is $1 \times 10^{-6} \text{ sec}^{-1}$.

(b) As in (a) except for the ERA reanalysis.

Figure 3. Longitude-Time plot of the NCEP reanalysis 200 hPa monthly mean vorticity anomaly from 1958 through 1996 averaged from 10N to 20N. Contour interval is $3 \times 10^{-5} \text{ sec}^{-1}$.

Figure 4. (a) Longitude-Time plot of the NCEP reanalysis 200 hPa monthly mean vorticity anomaly from 1979 through 1993 averaged from 10N to 20N. Contour interval is $3 \times 10^{-5} \text{ sec}^{-1}$.

(b) As in (a) except for the ERA reanalysis.

Figure 5. (a) Longitude-Time plot of the CCM3 200 hPa monthly mean divergence anomaly from 1979 through 1993 averaged from 5S to 5N. Contour interval is $1 \times 10^{-6} \text{ sec}^{-1}$.

(b) Longitude-Time plot of the CCM3 200 hPa monthly mean vorticity anomaly from 1979 through 1993 averaged from 10N to 20N. Contour interval is $3 \times 10^{-5} \text{ sec}^{-1}$.

Figure 6. (a) Longitude-Time plot of the CSM 200 hPa monthly mean divergence anomaly for model years 16 through 35 averaged from 5S to 5N. Contour interval is $1 \times 10^{-6} \text{ sec}^{-1}$.

(b) As in (a) except for model years 36 through 55.

(c) As in (a) except for model years 80 through 99.

(d) As in (a) except for model years 100 through 119.

Figure 7. (a) Longitude-Time plot of the CSM 200 hPa monthly mean vorticity anomaly for model years 16 through 35 averaged from 10N to 20N. Contour interval is $3 \times 10^{-5} \text{ sec}^{-1}$.

(b) As in (a) except for model years 36 through 55.

(c) As in (a) except for model years 80 through 99.

(d) As in (a) except for model years 100 through 119.

Figure 8. (a) Mean 200 hPa vorticity for the NCEP reanalysis for the period 1979 through 1993. Contour interval is $0.75 \times 10^{-5} \text{ sec}^{-1}$

(b) Harmonic dial for the first harmonic of the 200 hPa vorticity for the NCEP reanalysis for the period

1979 through 1993. The convention is that pointing north indicates a maximum in January with the progression through the year going clockwise. The scale for $5 \times 10^{-5} \text{ s}^{-1}$ is shown on the plot.

(c) As in (a) except for the ERA reanalysis.

(d) As in (b) except for the ERA reanalysis and what is plotted is the **difference** obtained from subtracting the NCEP values from the ERA. The scale for $2.5 \times 10^{-5} \text{ s}^{-1}$ is shown on the plot. This scale is half of that in (b).

(e) As in (a) except for the CCM3.

(f) As in (d) except for the CCM3 .

(g) As in (a) except for the CSM model years 16 to 35.

(h) As in (d) except for the CSM model years 16 to 35.

Figure 9. (a) Annual cycle for 200 hPa vorticity for 130E, 50N for NCEP reanalysis, 1958-1977, and 1977-1996 (thin solid lines), 1958-1996 (thick solid line), ERA reanalysis, 1979-1994 (thick dashed line), CCM3 1979-1993 (dash-dot line), CSM for 16-35, 35-55, 80-99, and 100-119 (thin dashed lines).

Vorticity units are in s^{-1} .

(b) As in (a) except for 270E, 20N.

(c) As in (a) except for 270E, 40N.

(d) As in (a) except for 300E, 50N.

(e) As in (a) except for 350E, 10N.

Figure 10.(a) Mean 200 hPa divergence for the NCEP reanalysis for the period 1979 through 1993. Contour interval is $1 \times 10^{-6} \text{ sec}^{-1}$

(b) Harmonic dial for the first harmonic of the 200 hPa divergence for the NCEP reanalysis for the period 1979 through 1993. The convention is that pointing north indicates a maximum in January with the progression through the year going clockwise. The scale for $10 \times 10^{-6} \text{ s}^{-1}$ is shown on the plot.

(c) As in (a) except for the ERA reanalysis.

(d) As in (b) except for the ERA reanalysis and what is plotted is the **difference** obtained from subtracting the NCEP values from the ERA. The scale for $10 \times 10^{-6} \text{ s}^{-1}$ is shown on the plot. This scale is equal to of that in (b).

(e) As in (a) except for the CCM3.

(f) As in (d) except for the CCM3 .

(g) As in (a) except for the CSM model years 16 to 35.

(h) As in (d) except for the CSM model years 16 to 35.

Figure 11. (a) Annual cycle for 200 hPa divergence for 120E, 5S-5N for NCEP reanalysis, 1958-1977, and 1977-1996 (thin solid lines), 1958-1996 (thick solid line), ERA reanalysis, 1979-1994 (thick dashed line), CCM3 1979-1993 (dash-dot line), CSM for 16-35, 35-55, 80-99, and 100-119 (thin dashed lines).

Divergence units are in s^{-1} .

(b) As in (a) except for averaged over the oceanic warm pool, 140-170E, 10S-10N.

(c) As in (a) except for 240E, 10N.

(d) As in (a) except for 270E, 40N.

(e) As in (a) except for 60E, 10S

(f) As in (a) except for 90E, 10S

Figure 12. Standard deviation of the monthly anomaly of 200 hPa relative vorticity. (a) NCEP, (b) ERA, (c) CCM3, (d) CSM years 100-119. Contour interval is $0.2 \times 10^{-5} s^{-1}$.

Figure 13. Standard deviation of the time series of 200 hPa vorticity with the seasonal cycle removed and filtered with the Trenberth(1988) 11 point filter to remove variations of less than 8 months. (a) NCEP, (b) ERA, (c) CCM3, (d) CSM years 100-119. Contour interval is $0.1 \times 10^{-5} s^{-1}$

Figure 14. Standard deviation of the monthly anomaly of 200 hPa divergence. (a) NCEP, (b) ERA, (c) CCM3, (d) CSM years 100-119. Contour interval is $0.4 \times 10^{-6} sec^{-1}$.

Figure 15. Standard deviation of the time series of 200 hPa divergence with the seasonal cycle removed and filtered with the Trenberth(1988) 11 point filter to remove variations of less than 8 months. (a) NCEP, (b) ERA, (c) CCM3, (d) CSM years 100-119. Contour interval is $0.4 \times 10^{-6} sec^{-1}$.